The Plant Cell, Vol. 27: 1999–2015, July 2015, www.plantcell.org

Arabidopsis *MAS2*, an Essential Gene That Encodes a Homolog of Animal NF-κ B Activating Protein, Is Involved in 45S Ribosomal DNA Silencing

Ana Belén Sánchez-García,[1] Verónica Aguilera,[1,2] Rosa Micol-Ponce, Sara Jover-Gil, and María Rosa Ponce[3]

Instituto de Bioingeniería, Universidad Miguel Hernández, 03202 Elche, Alicante, Spain

ORCID IDs: 0000-0002-1315-8400 (A.B.S.-G.); 0000-0003-3885-6624 (V.A.); 0000-0001-9389-2906 (R.M.-P.); 0000-0003-0770-4230 (M.R.P.)

Ribosome biogenesis requires stoichiometric amounts of ribosomal proteins and rRNAs. Synthesis of rRNAs consumes most of the transcriptional activity of eukaryotic cells, but its regulation remains largely unclear in plants. We conducted a screen for ethyl methanesulfonate-induced suppressors of *Arabidopsis thaliana ago1-52*, a hypomorphic allele of *AGO1* (*ARGONAUTE1*), a key gene in microRNA pathways. We identified nine extragenic suppressors as alleles of *MAS2* (*MORPHOLOGY OF AGO1-52 SUPPRESSED2*). Positional cloning showed that *MAS2* encodes the putative ortholog of NKAP (NF-κ B activating protein), a conserved eukaryotic protein involved in transcriptional repression and splicing in animals. The *mas2* point mutations behave as informational suppressors of *ago1* alleles that cause missplicing. *MAS2* is a single-copy gene whose insertional alleles are embryonic lethal. In yeast two-hybrid assays, MAS2 interacted with splicing and ribosome biogenesis proteins, and fluorescence in situ hybridization showed that MAS2 colocalizes with the 45S rDNA at the nucleolar organizer regions (NORs). The artificial microRNA *amiR-MAS2* partially repressed *MAS2* and caused hypomethylation of 45S rDNA promoters as well as partial NOR decondensation, indicating that MAS2 negatively regulates 45S rDNA expression. Our results thus reveal a key player in the regulation of rRNA synthesis in plants.

INTRODUCTION

The regulation of eukaryotic gene expression involves multiple precisely controlled and coordinated transcriptional and post-transcriptional processes. For example, nuclear rRNA genes are tightly regulated, as transcription of rRNAs involves a vast amount of cell resources, representing ~50% of transcription in many eukaryotic cells (reviewed in Grummt, 2003). Assembly of the ribosome requires stoichiometric amounts of rRNAs and ribosomal proteins (Laferté et al., 2006). *Arabidopsis thaliana* contains ~1000 tandemly arrayed copies of the 5S rRNA gene and 570 to 750 copies of the 45S rRNA gene per haploid genome (Layat et al., 2012). Not all rRNA genes are transcribed at a given cell; active genes are enriched in euchromatin and silenced genes in heterochromatin (Lawrence et al., 2004). Transcription of the genes in rDNA depends on the action of enzymes that regulate histone methylation and acetylation, DNA methylation, and nucleosome positioning (Layat et al., 2012).

In humans, the NF-κ B activating protein (NKAP) activates nuclear factor-κ B (Chen et al., 2003) and is a component of the Notch corepressor complex (Pajerowski et al., 2009). NOTCH proteins are transmembrane receptors involved in several conserved pathways that regulate cellular differentiation, proliferation, and apoptosis in animals (Bray, 2006). Human NKAP has also been found bound to different spliceosomal complexes (Jurica and Moore, 2002; Bessonov et al., 2008, 2010; Ilagan et al., 2013) and to pre-mRNAs and spliced mRNAs (Burgute et al., 2014). A role has been proposed for human NKAP in regulating constitutive splicing. NKAP interacts with several RNA binding proteins, including splicing factors; it binds to exons in pre-mRNAs as well as to small nuclear RNAs, small nucleolar RNAs, rRNAs, and long intergenic noncoding RNAs. *XIST* (*X-inactive-specific transcript*) regulatory RNA, the major effector of X chromosome epigenetic inactivation, has also been found bound to NKAP (Burgute et al., 2014).

NKAP is a conserved eukaryotic protein that was first discovered in *Caenorhabditis elegans* and named E01A2.4 or LET-504 (Howell and Rose, 1990). Based on the interactions of its mutant alleles and their effects on vulvar development, *let-504* was classified as a class B Synthetic Multivulva (SynMuv) gene (Poulin et al., 2005); genes of this class encode proteins involved in epigenetic repression of gene expression (Saffer et al., 2011). The NKAP family is defined by the presence of a domain that was initially named DUF926 and later SynMuv.

One posttranscriptional regulatory mechanism is mediated by microRNAs, a class of eukaryotic endogenous small RNAs (20 to 24 nucleotides) that modulate a wide variety of processes (Jones-Rhoades et al., 2006; Bartel, 2009; Voinnet, 2009). Plant microRNAs play their regulatory role in the cytoplasm, through their selective loading into an ARGONAUTE (AGO) protein, the best known of which is AGO1 (Bartel, 2009; Mallory and Vaucheret, 2010). AGO proteins form the core component of RNA-induced silencing complexes (Voinnet, 2009; Rogers and Chen, 2013).

Here, we describe a characterization of *MORPHOLOGY OF AGO1-52 SUPPRESSED2* (*MAS2*), the Arabidopsis putative

[1] These authors contributed equally to this work.
[2] Current address: Centro Nacional de Biotecnología, Consejo Superior de Investigaciones Científicas, 28049 Madrid, Spain.
[3] Address correspondence to mrponce@umh.es.
The author responsible for distribution of materials integral to the findings presented in this article in accordance with the policy described in the Instructions for Authors (www.plantcell.org) is: María Rosa Ponce (mrponce@umh.es).
www.plantcell.org/cgi/doi/10.1105/tpc.15.00135

ortholog of human *NKAP*. We isolated 11 *mas2* alleles, nine of which behave as informational suppressors of two hypomorphic *ago1* alleles that exhibit missplicing. We found *MAS2* to be an essential gene whose protein product colocalizes with and regulates expression of the 45S rDNA.

RESULTS

The *mas2-1* Mutation Is an Extragenic Suppressor of *ago1-52*

We previously isolated and studied *ago1-52* (Berná et al., 1999; Jover-Gil et al., 2005; Jover-Gil et al., 2012), a hypomorphic, viable allele of *AGO1*. To study the regulation, action, and interactions of *AGO1*, we conducted a genetic screen to identify ethyl methanesulfonate (EMS)-induced second-site mutations suppressing the morphological phenotype of *ago1-52*; we termed these extragenic suppressors *morphology of argonaute1-52 suppressed* (*mas*) mutations (Micol-Ponce et al., 2014). One of the lines isolated was given the P2 11.1 protocol number and carried a suppressor mutation that we named *mas2-1*.

The *ago1-52* mutant exhibits a pleiotropic phenotype, consisting of leaves with no clear boundary between petiole and lamina, partial loss of adaxial-abaxial polarity in leaves and floral organs, compact inflorescences, moderately low fertility, slow growth, reduced plant size and number of vegetative leaves, and late flowering (Jover-Gil et al., 2012; Micol-Ponce et al., 2014). The *ago1-52 mas2-1* plants were closer in phenotype to the wild-type Landsberg *erecta* (L*er*) than to the *ago1-52* mutant. In these double mutant plants, we observed a clear boundary between leaf lamina and petiole (Figures 1A to 1D). Also, their growth rate, height, flowering time, and fertility were intermediate between those of *ago1-52* and L*er*, and their general body architecture, inflorescences, and fruits looked almost wild type (Figures 1E to 1I).

To reduce the number of EMS-induced mutations, we backcrossed P2 11.1 twice to L*er*. In the progeny of these backcrosses, the *mas2-1* mutation did not cause any visible phenotype on its own in an *AGO1/AGO1* background (Figure 1B), and its suppressor effect seemed to be dominant.

MAS2 Encodes the Putative Arabidopsis Ortholog of Human NKAP

To identify the *MAS2* gene, we subjected the *ago1-52 mas2-1* (P2 11.1) double mutant to iterative linkage analysis (Supplemental Table 1), as previously described (Ponce et al., 1999, 2006). The results indicated that *mas2-1* is a dominant mutation that maps to the upper telomere of chromosome 4, within a 157-kb candidate region encompassing 39 annotated genes (Supplemental Figure 1). A G→A mutation in the coding region of one of the candidate genes, At4g02720, was present in *ago1-52 mas2-1* plants but absent from L*er* and *ago1-52* plants (Supplemental Figure 2).

At4g02720 is an intronless, single-copy gene that encodes a protein of 422 amino acids, which contains the SynMuv domain characteristic of NKAP family members. The G→A mutation

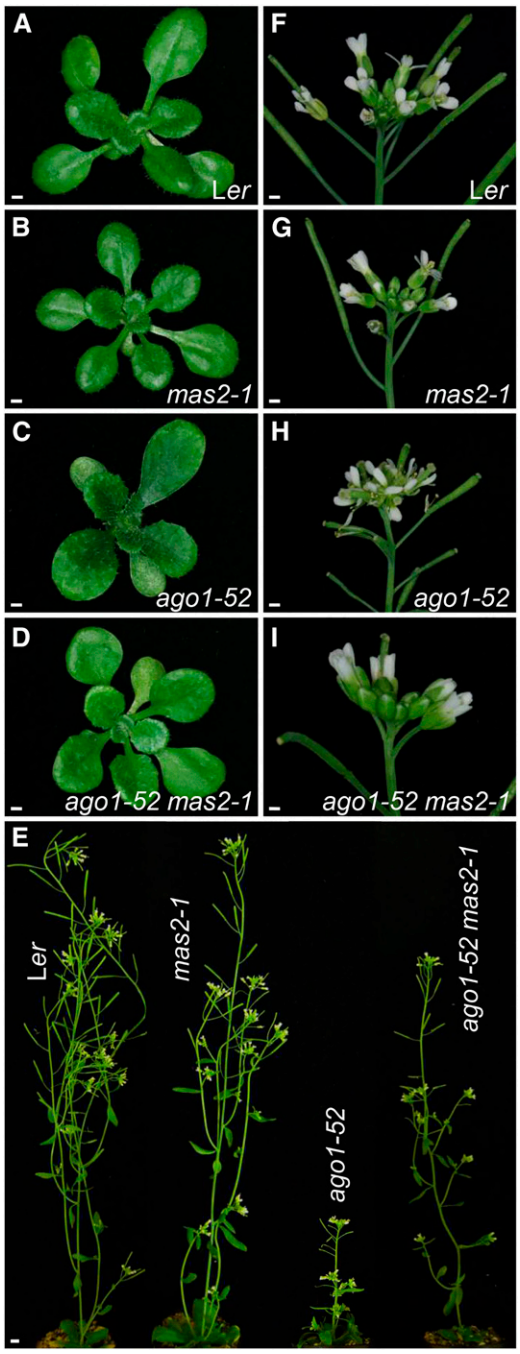

Figure 1. Suppression of the Phenotype of *ago1-52* by *mas2-1*.

(A) to **(D)** Rosettes of L*er* **(A)**, *mas2-1* **(B)**, *ago1-52* **(C)**, and *ago1-52 mas2-1* **(D)** plants.
(E) Adult plants of L*er*, *mas2-1*, *ago1-52*, and *ago1-52 mas2-1*.
(F) to **(I)** Inflorescences of L*er* **(F)**, *mas2-1* **(G)**, *ago1-52* **(H)**, and *ago1-52 mas2-1* **(I)** plants.
Pictures were taken at 21 (**[A]** to **[D]**) and 48 **(E)** DAS. Bars = 1 mm **(A)** to **(D)** and **(F)** to **(I)** and 1 cm in **(E)**.

carried by *mas2-1* is predicted to cause an Ala312→Trp substitution within the SynMuv domain (Figure 2). We also sequenced At4g02720 in the remaining 22 suppressor lines that we isolated, finding that nine of them bore additional *mas2* alleles, which we named *mas2-4* to *mas2-11*. All these alleles, except *mas2-11*, carry missense mutations mapping to a narrow (32 bp) region of At4g02720 encoding the SynMuv domain (Figure 2A; Supplemental Figure 2). Such a large allelic series found in a single genetic screen strongly supports the hypothesis that At4g02720 (hereafter, *MAS2*) is the causal gene for the suppression of the phenotype of *ago1-52* exhibited by P2 11.1.

All EMS-Induced *mas2* Alleles Carry Point Mutations Affecting Conserved Regions of MAS2

To ascertain whether the *mas2* mutations affect residues conserved among NKAP family members, we aligned MAS2 with other NKAP proteins. Full-length MAS2 has 32.4% identity to human NKAP, 30.0% to *Drosophila melanogaster* CG6066, and 33.5% to *C. elegans* LET-504. The SynMuv domain, which is 109 amino acids in the human NKAP, showed sequence similarities of 81 to 82%. By selecting putative NKAPs from a single representative of each of the supergroups identified in recent phylogenies based on massive sequencing (He et al., 2014), we only found conservation in the SynMuv domain: Its identity was 43.2% between Arabidopsis and the fungus *Mucor circinelloides* and 57.8% between *Homo sapiens* and the protozoan *Eimeria mitis*. All *mas2* mutations, except *mas2-11*, affected SynMuv domain residues that were highly conserved among all eukaryotes (Figures 2B and 2C; Supplemental Figure 3).

We also found very high conservation in a multiple alignment of several angiosperm NKAPs, to which we added that of the moss *Physcomitrella patens*: Only four of the 106 amino acids of the SynMuv domain differed between Arabidopsis and *P. patens* or rice (*Oryza sativa*). We detected a short conserved region, at the N terminus of MAS2 (residues 42 to 68), to which the *mas2-11* mutation maps (Pro64→Leu; Figure 2B; Supplemental Figure 4). The latter domain seems to be unique to moss and chlorophyta, as animals, red algae, and protists lack this domain. The conservation of this region suggests its relevance for NKAP function in plants.

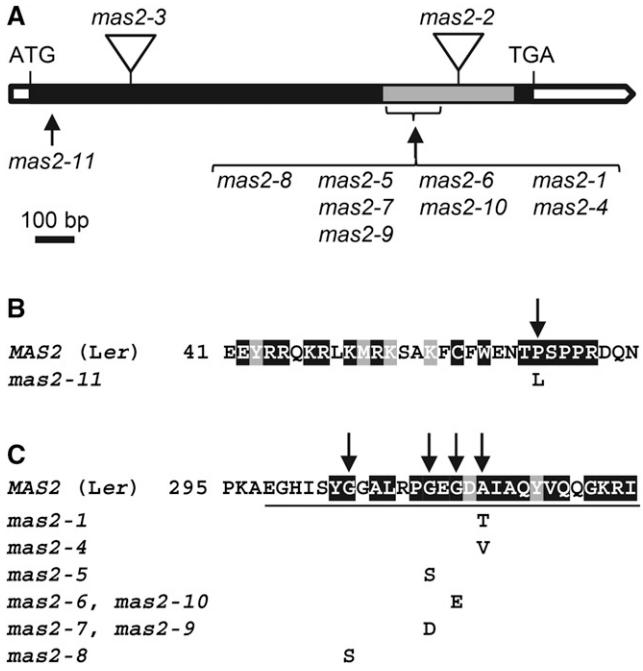

Figure 2. *MAS2* Gene Structure and Alleles.

(A) Schematic representation of the *MAS2* (At4g02720) gene, showing the nature and position of the *mas2* mutant alleles. White and black boxes represent untranslated and coding regions, respectively. The region encoding the SynMuv domain is shown in gray. Arrows indicate nucleotide substitutions, and triangles indicate T-DNA insertions.
(B) and **(C)** Predicted effects of the *mas2* mutations on the MAS2 protein. Residues conserved among plants **(B)** or eukaryotes **(C)** are shaded black (identical) and gray (similar). The full-length alignments are shown in Supplemental Figures 3 and 4. The amino acids underlined belong to the SynMuv domain.

mas2-1 Suppresses the Phenotype of Two *ago1* Alleles That Exhibit Missplicing

To ascertain if suppression of *ago1-52* by *mas2-1* is allele specific, we crossed *mas2-1* single mutant plants to the *ago1-25*, *ago1-27* (Morel et al., 2002), and *ago1-51* (Jover-Gil et al., 2012) single mutants. Both *ago1-25* and *ago1-27* carry missense mutations, whereas *ago1-51* and *ago1-52* exhibit missplicing of the *AGO1* pre-mRNA (Supplemental Figure 5).

The *ago1-25 mas2-1* and *ago1-27 mas2-1* double mutants were indistinguishable from their *ago1-25* and *ago1-27* single mutant F2 siblings (Figures 3A to 3D). By contrast, the *ago1-51 mas2-1* double mutant exhibited suppression, though to a lesser extent than that seen in *ago1-52 mas2-1* plants (Figures 3E to 3H). For example, one of the most conspicuous traits of hypomorphic *ago1* mutants, the absence of a well-defined petiole (Jover-Gil et al., 2012), is suppressed in *ago1-51 mas2-1* leaves. In addition, *ago1-51 mas2-1* plants were slightly taller than the *ago1-51* plants, but the inflorescences and fruits of the double mutant were less compact and longer, respectively, than those of *ago1-51* (Supplemental Figure 6). These results indicate that *mas2-1* suppresses the mutant phenotype of *ago1-51* and *ago1-52*, which carry mutations causing missplicing, but not those of *ago1-25* and *ago1-27*, which carry missense mutations.

The *mas2* Mutations Modify the Ratio between Splice Variants from *ago1-51* and *ago1-52*

The G→A transition carried by *ago1-51* and *ago1-52* (Supplemental Figure 5) causes missplicing. Two abnormal splice forms are detectable by RT-PCR from *ago1-51* mRNA: The short splice form (*ago1-51.1*) is 3468 nucleotides long and lacks the last 39 nucleotides of the 7th exon and the 7th intron, and the long form (*ago1-51.2*) is 3578 nucleotides long and includes the entire 7th intron. Translation of the short splice form should produce an AGO1 protein similar to wild type but lacking

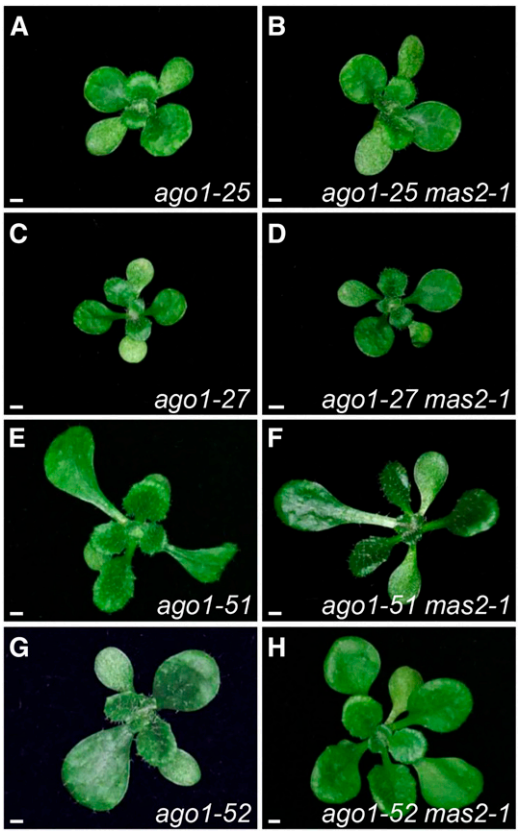

Figure 3. Genetic Interactions of *mas2-1* with *ago1-25*, *ago1-27*, *ago1-51*, and *ago1-52*.

Rosettes of *ago1-25* **(A)**, *ago1-25 mas2-1* **(B)**, *ago1-27* **(C)**, *ago1-27 mas2-1* **(D)**, *ago1-51* **(E)**, *ago1-51 mas2-1* **(F)**, *ago1-52* **(G)**, and *ago1-52 mas2-1* **(H)** plants. Pictures were taken at 21 DAS. Bars = 1 mm.

13 amino acids of the PAZ domain, but translation of the long splice form should produce a truncated protein. A single splice form of *AGO1* was detected from *ago1-52* RNA; this form is 3517 nucleotides long and includes 10 nucleotides of the 20th intron (Jover-Gil et al., 2012).

The *mas2-1* mutation suppresses the morphological phenotype of *ago1-51* and *ago1-52*; therefore, we wondered if *mas2-1* modifies the number and/or relative amounts of *AGO1* splice variants in these *ago1* mutants. We designed PCR primers to amplify the wild type (abbreviated as *wAGO1*) and mutant (*ago1-51.1*, *ago1-51.2*, and *ago1-52*) splice forms (Supplemental Table 2). Using primers designed to amplify all possible splice forms (total *AGO1* mRNAs, abbreviated as *tAGO1*), we could not detect the *wAGO1* splice form in *ago1-51* plants by RT-PCR, as previously reported (Jover-Gil et al., 2012) (Supplemental Figure 7A). However, using primers that selectively amplify *wAGO1*, we did detect this splice form at a very low level in the *ago1-51* mutant (Supplemental Figure 7A). We confirmed the presence of the *wAGO1*, *ago1-51.1*, and *ago1-51.2* mRNA variants by reverse transcription and quantitative PCR (RT-qPCR). These results indicated that the *wAGO1* splice form represents 0.8 and 2.1% of *tAGO1* in *ago1-51* and *ago1-51 mas2-1* plants, respectively (Figure 4A).

We also detected *wAGO1* in *ago1-52* and *ago1-52 mas2-1* plants by RT-PCR using specific primers (Supplemental Figure 7B and Supplemental Table 2) and found by RT-qPCR that *wAGO1* represents 2.5 and 14.8% of *tAGO1* in *ago1-52* and *ago1-52 mas2-1*, respectively (Figure 4B).

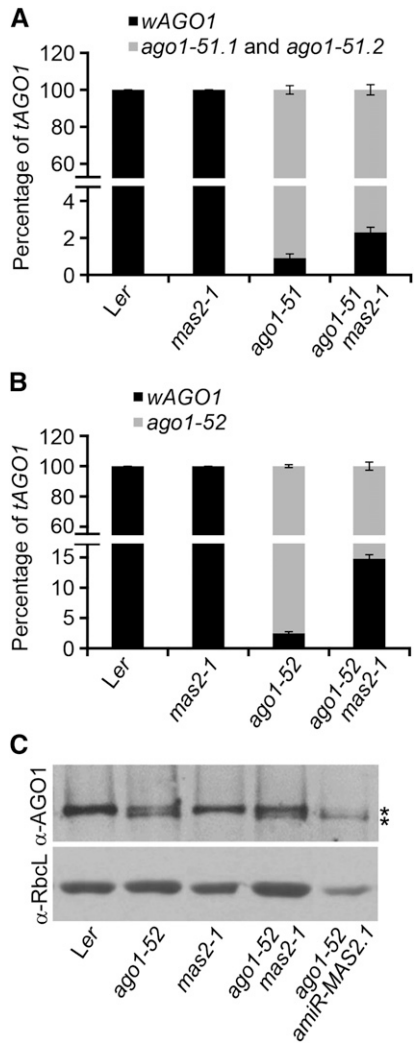

Figure 4. Effects of *mas2-1* on the Levels of *ago1-51* and *ago1-52* mRNA and Protein Products.

(A) and **(B)** RT-qPCR analyses using primers to amplify all of the splice forms of *AGO1* (*tAGO1*) or specifically the wild-type *AGO1* mRNA (*wAGO1*). The percentages of *wAGO1* and the mutant splice forms with respect to *tAGO1* were estimated in L*er*, *mas2-1*, *ago1-51*, and *ago1-51 mas2-1* plants **(A)** and in L*er*, *mas2-1*, *ago1-52*, and *ago1-52 mas2-1* plants **(B)**.

(C) Detection of AGO1 proteins by immunoblot using a primary antibody against AGO1 (α-AGO1). Total proteins from L*er*, *mas2-1*, *ago1-52*, *ago1-52 mas2-1*, and *ago1-52 amiR-MAS2.1* plants were used. Asterisks indicate the AGO1 (upper band) and the AGO1-52 (lower band) proteins. α-RbcL was used as the loading control.

To study the effects of *mas2-4* to *mas2-11* on the splicing of *ago1-52* in all the *ago1-52 mas2* lines isolated in our screen, we used RT-qPCR to measure the ratio between the *wAGO1* and *ago1-52* splice forms, which remained as in *ago1-52 mas2-1*. The only exception was the P1 5.33 (*ago1-52 mas2-5*) line, in which the ratio was the same as in the *ago1-52* mutant (Supplemental Figure 7C).

The *mas2* Mutations Modify the Ratio between Protein Variants Encoded by *ago1-51* and *ago1-52*

The increased *wAGO1* level we observed in *ago1-51 mas2-1* and *ago1-52 mas2-1* plants compared with *ago1-51* and *ago1-52*, respectively, seemed to be too modest to explain the strong phenotypic suppression observed. Hence, we performed immunoblot assays using an α-AGO1 antibody, extracting proteins from plants carrying different *ago1* alleles: the null *ago1-2* (Bohmert et al., 1998) and the hypomorphic *ago1-25*, *ago1-27* (Morel et al., 2002), *ago1-51*, and *ago1-52* (Jover-Gil et al., 2012) alleles. As expected, we detected no AGO1 protein in the *ago1-2* mutant; a single protein of ~130 kD in *ago1-25* and *ago1-27*, likely the AGO1-25 and AGO1-27 proteins, respectively; and ~130- and ~60-kD proteins in *ago1-51* plants, likely the AGO1-51.1 and AGO1-51.2 mutant proteins, respectively (Supplemental Figure 8). Due to the difference between the wild-type (AGO1) and the AGO1-51.1 protein, which is only 13 amino acids smaller than AGO1, we could not discriminate them in immunoblots. The largest amount of protein corresponded to the ~130-kD band, while the ~60-kD band was very weak (Supplemental Figure 8), suggesting that the truncated AGO1-51.2 protein is degraded or is less translatable than AGO1-51.1 or the wild-type protein. In *ago1-52* plants, two different proteins were also detected: one of ~130 kD, the size of the wild-type AGO1 protein, and another of ~125 kD, likely the AGO1-52 protein (Figure 4C; Supplemental Figure 8). Both AGO1 and AGO1-52 proteins were present in similar amounts in *ago1-52* (Figure 4C; Supplemental Figure 8), which suggests a greater translatability of the wild-type *AGO1* splice form compared with the *ago1-52* form or a higher stability of AGO1 protein.

These results suggest that *mas2-1* suppresses the phenotypes of *ago1-51* and *ago1-52* by increasing the translatability of *wAGO1* mRNA and/or stability of AGO1 protein more than modifying the splicing of *ago1-51* and *ago1-52* mRNAs. This assumption is also consistent with our results with the other *mas2* suppressor alleles described above, because one of them (*mas2-5*) does not change the ratio between *wAGO1*/*ago1-52* splice forms in *ago1-52 mas2-5* plants.

Overexpression of *mas2-1*, but Not *MAS2*, Suppresses *ago1-52* and *ago1-51*

To further examine the effect of *mas2-1* on the phenotypes of *ago1-51* and *ago1-52*, and to compare the effects of the overexpression of the *MAS2* and *mas2-1* alleles in wild-type *AGO1*/*AGO1* and mutant *ago1*/*ago1* backgrounds, we generated $35S_{pro}$*:MAS2* and $35S_{pro}$*:mas2-1* constructs, which were transferred into L*er*, *ago1-51*, and *ago1-52* plants. The $35S_{pro}$*:MAS2*, $35S_{pro}$*:mas2-1*, and L*er* plants were indistinguishable (Supplemental Figures 9A to 9C), and the $35S_{pro}$*:MAS2* transgene did not suppress the mutant phenotype of *ago1-51* and *ago1-52* plants (Supplemental Figures 9E to 9H). By contrast, $35S_{pro}$*:mas2-1* suppressed the mutant phenotype of *ago1-52* (Supplemental Figures 9I and 10) and *ago1-51*. Suppression of *ago1-51* by *mas2-1* was stronger in the $35S_{pro}$*:mas2-1 ago1-51* transgenic plants (Supplemental Figures 9F and 11) than in the *ago1-51 mas2-1* double mutant (Figure 3F). These results reconfirm that *mas2-1* is a true extragenic suppressor of *ago1-51* and *ago1-52* and that it is antimorphic, rather than hypermorphic, as suggested by the absence of suppression seen in $35S_{pro}$*:MAS2 ago1* plants.

Insertional *mas2* Alleles Are Embryonic Lethal

We also searched for insertional alleles of *MAS2* and identified three publicly available lines. The GABI_318G03 line (Supplemental Figure 12A) was phenotypically wild type and not studied further. SAIL_335_C06, which we named *mas2-2*, is in the Col-3 background and carries a T-DNA insertion 1074 bp downstream of the translation start codon of At4g02720, in the region encoding the SynMuv domain (Figure 2A). We found no *mas2-2*/*mas2-2* homozygotes among 274 T4 genotyped plants. Aborted seeds accounted for 0.28% ± 0.97% of seeds (n = 353, n being the number of embryos from fertilized ovules) in the siliques from six *MAS2*/*MAS2* plants, where no unfertilized ovules were seen. By contrast, the siliques of six *MAS2*/*mas2-2* plants showed 29.78% ± 8.38% aborted seeds (n = 339) and 3.42% ± 4.68% unfertilized ovules (n = 351, n being the sum of the number of unfertilized ovules plus the number of embryos from fertilized ovules; Supplemental Figure 13).

We named the At4g02720 allele carried by CSHL_GT188551 (in a L*er* background) *mas2-3* and found the coding region in *mas2-3* is interrupted by a T-DNA insertion 233 bp downstream of the translation start codon (Figure 2A). We genotyped 31 CSHL_GT188551 plants, none of which was *mas2-3*/*mas2-3*. Aborted seeds were found in dissected siliques from five *MAS2*/*MAS2* (0.75% ± 1.3%; n = 532) and five *MAS2*/*mas2-3* plants (26.33% ± 5.19%; n = 433). No unfertilized ovules were found in the *mas2-3*/*MAS2* plants studied or in their *MAS2*/*MAS2* siblings. Taken together, these results suggest that *MAS2* is an essential gene whose null alleles are embryonic lethal.

Partial Silencing of *MAS2* by *amiR-MAS2* Causes a Pleiotropic Phenotype

The recessive embryonic lethality exhibited by the null *mas2-2* and *mas2-3* alleles, together with the likely antimorphic effects of the *mas2* suppressor mutations, prompted us to attempt to obtain viable plants with a partial loss of *MAS2* function. To this end, we designed and constructed a transgene carrying an artificial microRNA targeting At4g02720 ($35S_{pro}$*:amiR-MAS2*), which was transferred into wild-type Col-0, L*er*, and En-2 plants, producing 72, 15, and 13 independent T1 transformant lines, respectively. Among these transformants, we identified 10 (Col-0), 3 (L*er*), and 6 (En-2) plants with pointed and serrated leaves, to a greater or lesser extent (Supplemental Figure 14; Figure 5B). We analyzed by RT-qPCR the degree of *MAS2* silencing in several of these *amiR-MAS2* lines in the Col-0 background.

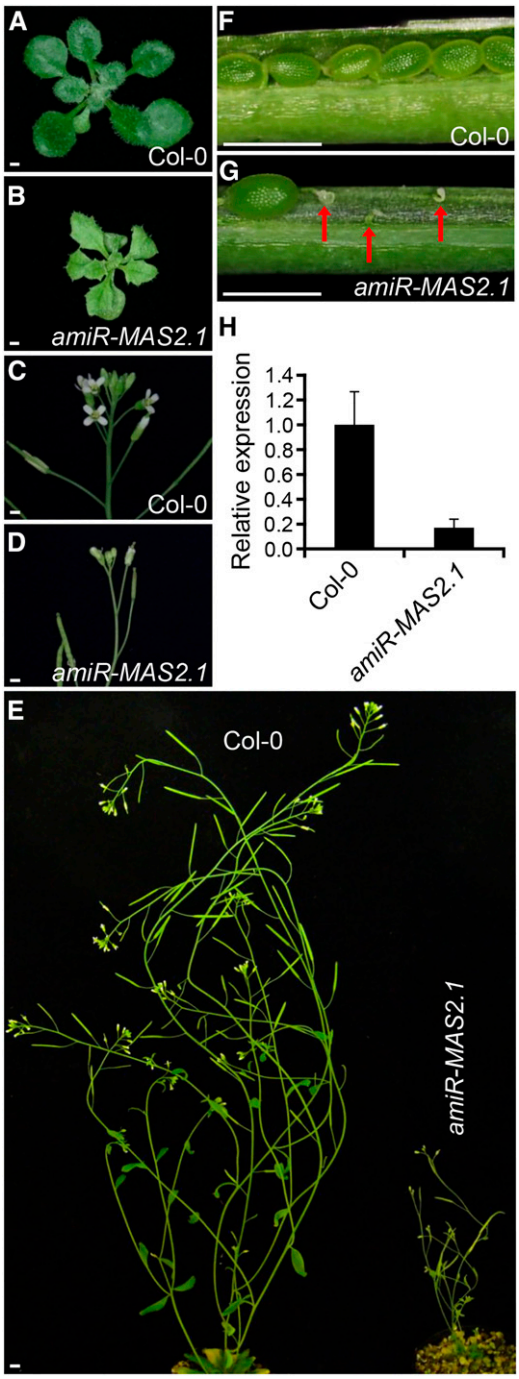

Figure 5. Phenotypic Effects of the *amiR-MAS2.1* Transgene in the Col-0 Background.

(A) and **(B)** Rosettes of Col-0 **(A)** and *amiR-MAS2.1* **(B)** (in the Col-0 background) plants.
(C) and **(D)** Inflorescences of Col-0 **(C)** and *amiR-MAS2.1* **(D)** plants.
(E) Adult Col-0 and *amiR-MAS2.1* plants.
(F) and **(G)** Dissected siliques from Col-0 **(F)** and *amiR-MAS2.1* **(G)** plants. Red arrows indicate unfertilized ovules.
(H) *MAS2* expression levels in Col-0 and *amiR-MAS2.1* plants. Three biological replicas with three technical replicas each were performed. Error bars represent standard deviations.

Pictures were taken at 21 (**[A]** and **[B]**) and 48 (**[C]** to **[G]**) DAS. Bars = 1 mm in **(A)** to **(D)**, **(F)**, and **(G)**, and 1 cm in **(E)**.

Homozygous plants of the line that we termed *amiR-MAS2.1* displayed the strongest mutant phenotype and also exhibited a 5-fold reduction of *MAS2* mRNA levels compared with the wild type (Figure 5H); these were chosen for further studies.

First- and third-node leaves of *amiR-MAS2.1* plants exhibited a vein pattern with reduced complexity (Supplemental Figures 15A to 15D), an increased number of air spaces in the palisade mesophyll (Supplemental Figures 15E to 15H), fewer vegetative leaves (7.82 ± 0.56 in *amiR-MAS2.1* and 12.87 ± 0.61 in Col-0, scored at 27 d after stratification [DAS]; $n \geq 47$), and early flowering (bolting was apparent in 51.3% of *amiR-MAS2.1* plants and 2.1% of Col-0 at 20 DAS; $n \geq 39$). These transgenic plants were also dwarfed, with thinner stems and fewer flowers than Col-0 (Figures 5A to 5E). We dissected siliques from 10 *amiR-MAS2.1* homozygous plants and found 18.46% ± 16.87% aborted seeds ($n = 260$) and 17.46% ± 23.05% unfertilized ovules ($n = 315$; Figure 5G).

The pleiotropic phenotype exhibited by *amiR-MAS2.1* plants suggests a role for *MAS2* in Arabidopsis development. In particular, *amiR-MAS2.1* leaves are reminiscent of the leaves of mutants carrying loss-of-function alleles of genes encoding ribosomal proteins (Van Lijsebettens et al., 1994; Ito et al., 2000; Creff et al., 2010; Horiguchi et al., 2011; Casanova-Sáez et al., 2014).

amiR-MAS2.1 Increases the Severity of the Mutant Phenotype of *ago1-52*

To study the effects of *MAS2* partial loss of function on the phenotype of *ago1-52*, we crossed *ago1-52/ago1-52* to *amiR-MAS2.1/amiR-MAS2.1* and sowed the F2 progeny on plates supplemented with hygromycin. Only two phenotypic classes of *ago1-52/ago1-52* plants were obtained: (1) lethal seedlings that only produced cotyledons and a few rod-like leaves (Figure 6C), which we inferred to be *ago1-52/ago1-52; amiR-MAS2.1/amiR-MAS2.1*; and (2) viable seedlings that developed into plants with narrow and strongly serrated leaves that exhibited fasciated stems and aberrant flowers (Figures 6D to 6H) and yielded few seeds, which we inferred to be *ago1-52/ago1-52; amiR-MAS2.1*. In the F3 and F4 progeny of the latter plants, a 3:1 (Hyg^r:Hyg^s) segregation was observed, confirming that they were homozygous for *ago1-52* but hemizygous for *amiR-MAS2.1*. The phenotype of the *ago1-52/ago1-52; amiR-MAS2.1/amiR-MAS2.1* lethal seedlings resembled that of plants homozygous for null alleles of *AGO1*, whereas the *ago1-52/ago1-52; amiR-MAS2.1* plants were very similar to those homozygous for the *ago1-103* mutation, a very strong but viable allele of *AGO1* (Fernández-Nohales et al., 2014).

We also quantified the percentage of *AGO1* mRNAs in the *ago1-52/ago1-52; amiR-MAS2.1/amiR-MAS2.1* lethal seedlings. In these plants, the *wAGO1* and *ago1-52* splice forms represented 0.7 and 99.3% of *tAGO1*, respectively (Supplemental Figure 16). The percentage of *wAGO1* in *ago1-52/ago1-52; amiR-MAS2.1/amiR-MAS2.1* (0.7%) is almost half of that found

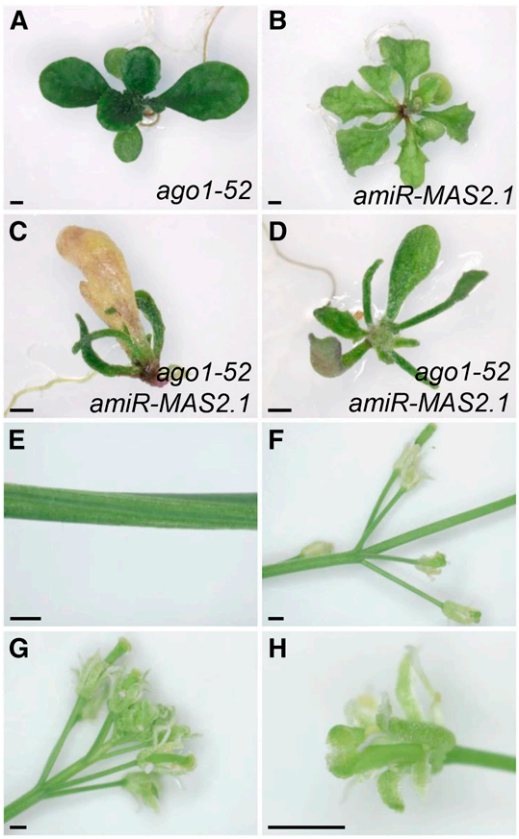

Figure 6. Phenotypic Effects of the *amiR-MAS2.1* Transgene in the *ago1-52* Background.

(A) to **(C)** Rosettes of *ago1-52/ago1-52* **(A)**, *amiR-MAS2.1/amiR-MAS2.1* **(B)**, and *ago1-52/ago1-52; amiR-MAS2.1/amiR-MAS2.1* **(C)** plants.
(D) to **(H)** Rosette **(D)**, stems (**[E]** and **[F]**), inflorescence **(G)**, and flower **(H)** of *ago1-52/ago1-52*; *amiR-MAS2.1* plants.
Pictures in **(A)** to **(D)** were taken at 21 DAS. Bars = 1 mm.

in *ago1-52* plants (1.2%) and could explain their extreme phenotype.

We also detected both the AGO1 and AGO1-52 proteins in the immunoblot assay of *ago1-52 mas2-1* and *ago1-52 amiR-MAS2.1* homozygous plants. The AGO1 protein was more abundant than AGO1-52 in *ago1-52 mas2-1* plants, whereas *ago1-52 amiR-MAS2.1* plants displayed an opposite pattern, with the AGO1-52 protein as the predominant variant (Figure 4C).

MAS2 Interacts in a Yeast Two-Hybrid Assay with Proteins Involved in Splicing and Translation

To better understand the function of MAS2, we decided to look for its interactors in a yeast two-hybrid (Y2H) assay. Two Arabidopsis cDNA libraries obtained from whole Arabidopsis plants, totaling 21 million prey clones, were used in the screening, which was performed at PanBioNet (http://www.panbionet.com). The bait contained the full-length coding region of *MAS2*. The screen identified 91 prey clones, representing 14 different genes, and these clones were confirmed by directed Y2H assays (Supplemental Table 3). These genes have not been previously studied in Arabidopsis, except for At1g20920, but their annotated functions are related to RNA processing and ribosome-related processes, as indicated by sequence similarity to known proteins.

Three of the interactors were related to ribosome biogenesis, including RPS24B, the second most represented interactor, which is one of the two Arabidopsis S24-type proteins in the 40S ribosomal subunit. Two other interactors, the putative ortholog of the Nucleolar protein 53 (NOP53) of *Saccharomyces cerevisiae* and RRNA-processing Protein 7 (RRP7), are nucleolar proteins involved in pre-rRNA processing and ribosome assembly in yeast (Granato et al., 2008).

The most represented interactor in the Y2H-based screen, in 23 of the 55 clones (Supplemental Table 3), was CAX INTERACTING PROTEIN4 (CXIP4), a protein of unknown function that was previously identified as interacting with the high-affinity vacuolar calcium antiporter CAX1 (Cheng et al., 2004). CXIP4 occurs exclusively in plants and 30 amino acids of its N-terminal region show 70% similarity to the mammalian splicing factor SREK1-interacting protein 1, as shown in the Aramemnon database (http://aramemnon.botanik.uni-koeln.de/index.ep; Schwacke et al., 2003). Other interactors were also involved in pre-mRNA splicing (Supplemental Table 3), including REGULATOR OF CBF GENE EXPRESSION1/RH42, a DEAD box RNA helicase (Guan et al., 2013).

The interaction between MAS2 and the protein encoded by At4g33690, annotated as an unknown protein, has also been found among the more than 6200 Y2H interactions included in the Arabidopsis interactome map (http://interactome.dfci.harvard.edu/A_thaliana/index.php; Arabidopsis Interactome Mapping Consortium, 2011).

Our results suggest a role for MAS2 in the regulation of pre-mRNA alternative splicing and translation. Our results also agree with those obtained with the mammalian NKAPs, which localize to nuclear speckles and interact with nuclear ribonuclear proteins, splicing factors, several RNA helicases, and other factors involved in the maturation of 45S pre-rRNA and ribosome biogenesis (Burgute et al., 2014).

MAS2 Expression and MAS2 Nuclear Localization

To determine the spatial expression pattern of *MAS2*, we generated a $MAS2_{pro}$*:GUS* construct in which the *MAS2* promoter drives the expression of the β-glucuronidase gene and transferred this construct into Col-0. Homozygous $MAS2_{pro}$*:GUS* plants were selected and used to detect GUS activity, which was found in roots, cotyledons, young vegetative and cauline leaves, stems, and flower buds (Supplemental Figure 17). GUS activity changed depending on the developmental stage, being more intense in seedlings and young plants; we did not detect GUS staining in vegetative leaves after bolting (48 DAS) or in fully expanded cauline leaves (Supplemental Figures 17F and 17H). Additionally, we performed RT-qPCR amplifications using cDNA from assorted organs of L*er* and Col-0 and found that *MAS2* was expressed in all the studied tissues at similar levels (Supplemental Figure 18).

To ascertain if MAS2 is nuclear, similar to all animal NKAP proteins already studied, we generated $35S_{pro}$*:MAS2:GFP* and

MAS2$_{pro}$*:MAS2:GFP* constructs, which we transformed into Col-0 and L*er* plants. As expected, we detected GFP signal in the nucleus for both constructs (Figure 7; Supplemental Figures 19A and 19B). MAS2 subcellular localization depended on the cell cycle: In cells with a high rate of nuclear division, such as those located at the root apex or emerging lateral roots, MAS2:GFP occurred in a diffuse pattern throughout the nucleus (Figures 7A to 7C). By contrast, in cells of the root elongation zone, MAS2:GFP was nuclear with an exclusion zone at the nucleolus (Supplemental Figure 20). Furthermore, MAS2:GFP had a punctuate distribution (Figures 7D to 7F; Supplemental Figure 20), which became more evident in differentiated cells where it appeared only in discrete foci in the nucleus (Figures 7G to 7I). These perinucleolar foci perfectly matched the heterochromatic chromocenters, which were visualized as bright fluorescent dots by 4',6-diamidino-2-phenylindole (DAPI) staining. These regions contain centromeric and other heterochromatic repeats, including those corresponding to silent rRNA 45S genes (Costa-Nunes et al., 2010). We obtained identical results with the *35S*$_{pro}$*:MAS2:GFP* and *MAS2*$_{pro}$*:MAS2:GFP* transgenes (Supplemental Figures 19A and 19B).

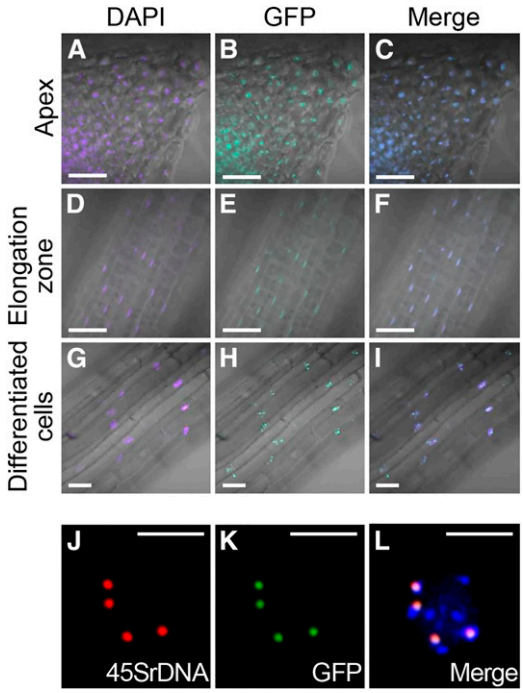

Figure 7. Subcellular Localization of the MAS2 Protein.

Confocal laser scanning microscopy of plants homozygous for the *35S*$_{pro}$*:MAS2:GFP* transgene.

(A) to **(I)** Different root zones from root apex (**[A]** to **[C]**), root elongation zone (**[D]** to **[F]**), and differentiated root cells (**[G]** to **[I]**). Fluorescence signals are DAPI (**[A]**, **[D]**, and **[G]**), GFP (**[B]**, **[E]**, and **[H]**), and their overlay (**[C]**, **[F]**, and **[I]**). Fluorescence and transmitted light contrast images were merged in **(A)** to **(I)**.

(J) to **(L)** Mitotic prophase nucleus from a flower bud cell showing the fluorescent signals from a hybridized 45S rDNA probe **(J)**, GFP **(K)**, and their overlay **(L)** with DAPI.

Bars = 30 μm in **(A)** to **(I)** and 50 μm in **(J)** to **(L)**.

To ascertain if the subcellular localization of MAS2 is modified by the *mas2-1* mutation, we generated the *MAS2*$_{pro}$*:mas2-1:GFP* construct, finding the fluorescent emission of MAS2-1:GFP indistinguishable from that of MAS2:GFP (Supplemental Figures 19C and 19D). These results indicate that overexpression of *MAS2* and the *mas2-1* mutation do not alter the nuclear localization of the MAS2 protein.

MAS2 Colocalizes with the 45S rDNA

In eukaryotes, tandem arrays of the genes encoding the four classes of nuclear rRNAs occur in different clusters. In the Arabidopsis Col-0 accession, the 5S rRNA genes occur within the pericentromeric heterochromatin of chromosomes 3, 4, and 5 (Campbell, 1992), and the 45S rRNA genes occur in the nucleolar organizer regions (NORs) at the tips of the short arms of the acrocentric chromosomes 2 and 4 (NOR2 and NOR4) (Lam et al., 2005; Layat et al., 2012). Transcription of the 5S rRNA gene by RNA polymerase III (Pol III) produces a 5S rRNA transcript (Cloix et al., 2002), and transcription of the 45S rRNA gene by RNA polymerase I (Pol I) produces a long polycistronic 45S pre-rRNA that is processed into the 5.8S, 18S, and 25S rRNA mature forms (Gruendler et al., 1989, 1991; Unfried et al., 1989).

The nuclear localization of MAS2 in discrete foci, together with the Y2H results, prompted us to analyze whether MAS2 colocalized with the 45S rRNA genes. To answer this question, we performed a fluorescence in situ hybridization (FISH) assays with plants expressing *35S*$_{pro}$*:MAS2:GFP*. In the root cells of these plants, the GFP signal perfectly matched the signal of a 45S rDNA probe (Sanchez Moran et al., 2001), indicating that MAS2 colocalizes with 45S rDNA (Figures 7J to 7L).

mas2-1 and *amiR-MAS2.1* Genetically Interact with *nuc-L1*

In Arabidopsis, *HISTONE DEACETYLASE6* (*HDA6*) and *NUCLEOLIN-LIKE PROTEIN1* (*NUC-L1*; also known as *PARALLEL1* [*PARL1*]) have been implicated in nuclear organization and transcriptional regulation of the 45S rDNA (Petricka and Nelson, 2007; Layat et al., 2012). The *amiR-MAS2.1* plants share some phenotypes, including reticulated and serrated leaves and altered leaf vein patterning, with the *nuc-L1* and *parl1* mutants and with mutants in genes encoding ribosomal proteins (Petricka and Nelson, 2007; Pontvianne et al., 2007).

Based on our interaction, localization, and phenotypic data for *MAS2*, we tested for a genetic interaction by crossing *mas2-1* and *amiR-MAS2.1* plants to the *parl1-2* nucleolin mutant (Petricka and Nelson, 2007). Although *mas2-1*/- plants show no morphological phenotype, the *mas2-1 parl1-2* double mutant plants displayed a synergistic phenotype, with small rosettes and pointed, serrated, and reticulated leaves resembling those of strong loss-of-function alleles of genes encoding ribosomal proteins (Van Lijsebettens et al., 1994; Ito et al., 2000; Creff et al., 2010; Horiguchi et al., 2011; Casanova-Sáez et al., 2014) (Figure 8E). Furthermore, the *mas2-1 parl1-2* double mutant had flowers with abnormal numbers of petals (5 to 6) and/or stamens (4 to 5), traits that we did not observe in either *mas2-1* or *parl1-2* single mutants (Figures 8J to 8L).

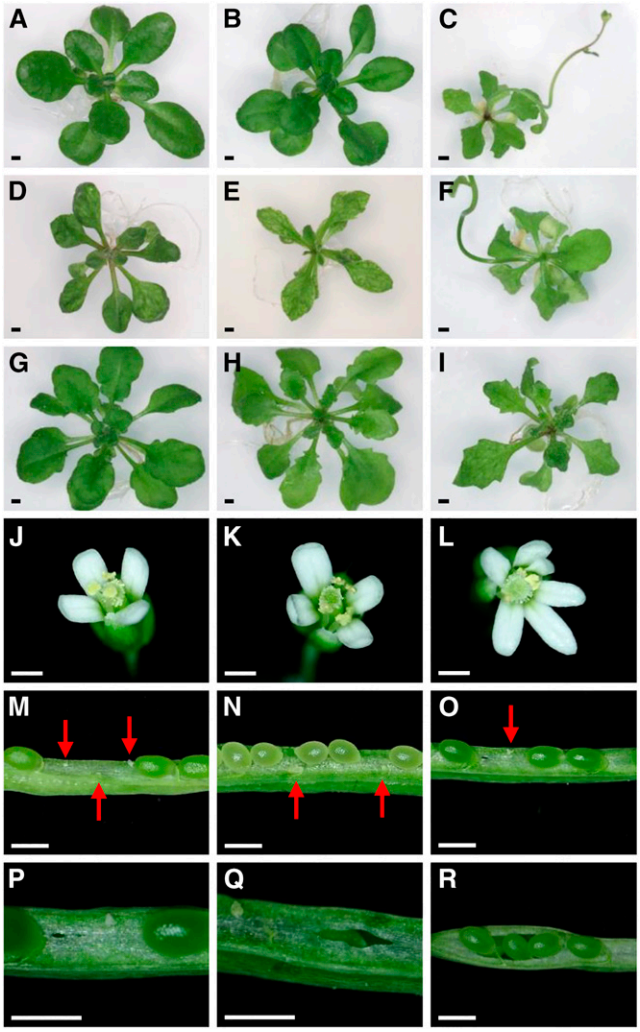

Figure 8. Genetic Interactions of *mas2-1* and *amiR-MAS2.1* with *parl1-2* and *hda6*.

(A) to **(I)** Rosettes of L*er* **(A)**, *mas2-1* **(B)**, *amiR-MAS2.1* **(C)**, *parl1-2* **(D)**, *mas2-1 parl1-2* **(E)**, *amiR-MAS2.1/amiR-MAS2.1; PARL1/parl1-2* **(F)**, *hda6-7* **(G)**, *mas2-1 hda6-7* **(H)**, and *amiR-MAS2.1 hda6-7* **(I)** plants.
(J) to **(L)** Flowers of *mas2-1* **(J)**, *parl1-2* **(K)**, and *mas2-1 parl1-2* **(L)** plants.
(M) to **(O)** Dissected siliques of *amiR-MAS2.1* **(M)**, *parl1-2* **(N)**, and *amiR-MAS2.1/amiR-MAS2.1; PARL1/parl1-2* **(O)** plants. Red arrows indicate unfertilized ovules.
(P) to **(R)** *amiR-MAS2.1/amiR-MAS2.1; PARL1/parl1-2* siliques exhibiting interrupted septa.
Pictures in **(A)** to **(I)** were taken at 28 DAS. Bars = 1 mm in **(A)** to **(I)** and 0.5 mm in **(J)** to **(R)**.

After genotyping 84 plants of different F2 and F3 families, we did not find any *amiR-MAS2.1/-; parl1-2/parl1-2* plant, and the *amiR-MAS2.1/amiR-MAS2.1; PARL1/parl1-2* and *amiR-MAS2.1/amiR-MAS2.1* plants were indistinguishable (Figures 8C and 8F). Since combined loss-of-function of *MAS2* and *PARL1* seemed to be lethal, we dissected siliques of *amiR-MAS2.1/amiR-MAS2.1*, *parl1-2/parl1-2*, and *amiR-MAS2.1/amiR-MAS2.1; PARL1/parl1-2* plants (Figures 8M to 8O), in which the unfertilized ovules and undeveloped seeds represented 42.9, 31.5, and 33.7% of the total, respectively. Moreover, around 25% of the siliques of *amiR-MAS2.1/amiR-MAS2.1; PARL1/parl1-2* plants displayed a disrupted septum between the two valves, a trait that we never observed in *amiR-MAS2.1/-* or *parl1-2/parl1-2* plants (Figures 8P to 8R). These results indicate that the combined loss of function of *MAS2* and *PARL1* is synergistic in *amiR-MAS2.1; PARL1/parl1-2* plants.

We also found that *mas2-1 hda6-7* leaves were strongly serrated (Figure 8H), suggesting that *HDA6* and *MAS2* are functionally related. The phenotype of *mas2-1 hda6-7* leaves is reminiscent of those of double mutants involving alleles of the *ASYMMETRIC LEAVES1* (*AS1*) or *AS2* genes and *axe1-5*, another loss-of-function allele of *HDA6* (Murfett et al., 2001). HDA6, AS1, and AS2 form a complex to repress *KNOX* genes and regulate leaf development (Luo et al., 2012). The morphological phenotype of *hda6-7* was hard to distinguish from the wild type in our growth conditions. The *amiR-MAS2.1/amiR-MAS2.1; hda6-7/hda6-7* and *amiR-MAS2.1/amiR-MAS2.1* plants were also indistinguishable (Figure 8I).

The phenotype of the *mas2-1 parl1-2* double mutant and, in particular, that of *amiR-MAS2.1/amiR-MAS2.1; PARL1/parl1-2* plants suggest that *MAS2* and *PARL1* are functionally related. The observation that both the *mas2-1* allele and the partial silencing of *MAS2* caused by *amiR-MAS2.1* synergistically interact with *parl1-2* reinforces the hypothesis that *mas2-1* is an antimorphic rather than a gain-of-function allele of *MAS2*.

amiR-MAS2.1 Alters Transcription of 45S rDNA, 45S Pre-rRNA Processing, and NOR Condensation

In Arabidopsis, each 45S rDNA unit has an intergenic spacer (IGS), two external transcribed spacers (ETSs), and the rRNA genes (18S, 5.8S, and 25S), which are separated by two internal transcribed spacers (ITSs) (Figure 9A). The IGS region separates adjacent genes and includes three repeat elements containing *Sal*I restriction sites that are separated by two spacer promoters, the promoter region, and the 5′ETS. The 3′ETS contains five repeated sequences (R1-R5) whose polymorphisms generate different variants of 45S rDNA genes (Abou-Ellail et al., 2011). The number of these variants differs among Arabidopsis accessions, with four (VAR1-VAR4) in Col-0 and other related accessions (Abou-Ellail et al., 2011). VAR2, VAR3, and VAR4 are expressed in Col-0 adult plants, while VAR1 is only expressed in germinating seeds or in mutants of genes involved in epigenetic regulation of the expression of 45S rDNA, such as *nuc-L1* and *hda6* (Pontvianne et al., 2010). We examined the expression of the 45S rDNA variants in *amiR-MAS2.1/amiR-MAS2.1* and *mas2-1/mas2-1* plants using p3/p4 primers (Figure 9A; Supplemental Table 2), which amplify the 3′ETS region of the 45S pre-rRNA and allow detection of all VAR variants (Pontvianne et al., 2010). RT-PCR amplifications showed no differences in the number or amount of rRNA variants between *amiR-MAS2.1/amiR-MAS2.1* and *mas2-1/mas2-1* plants and their respective backgrounds, Col-0 and L*er* (Figure 9B).

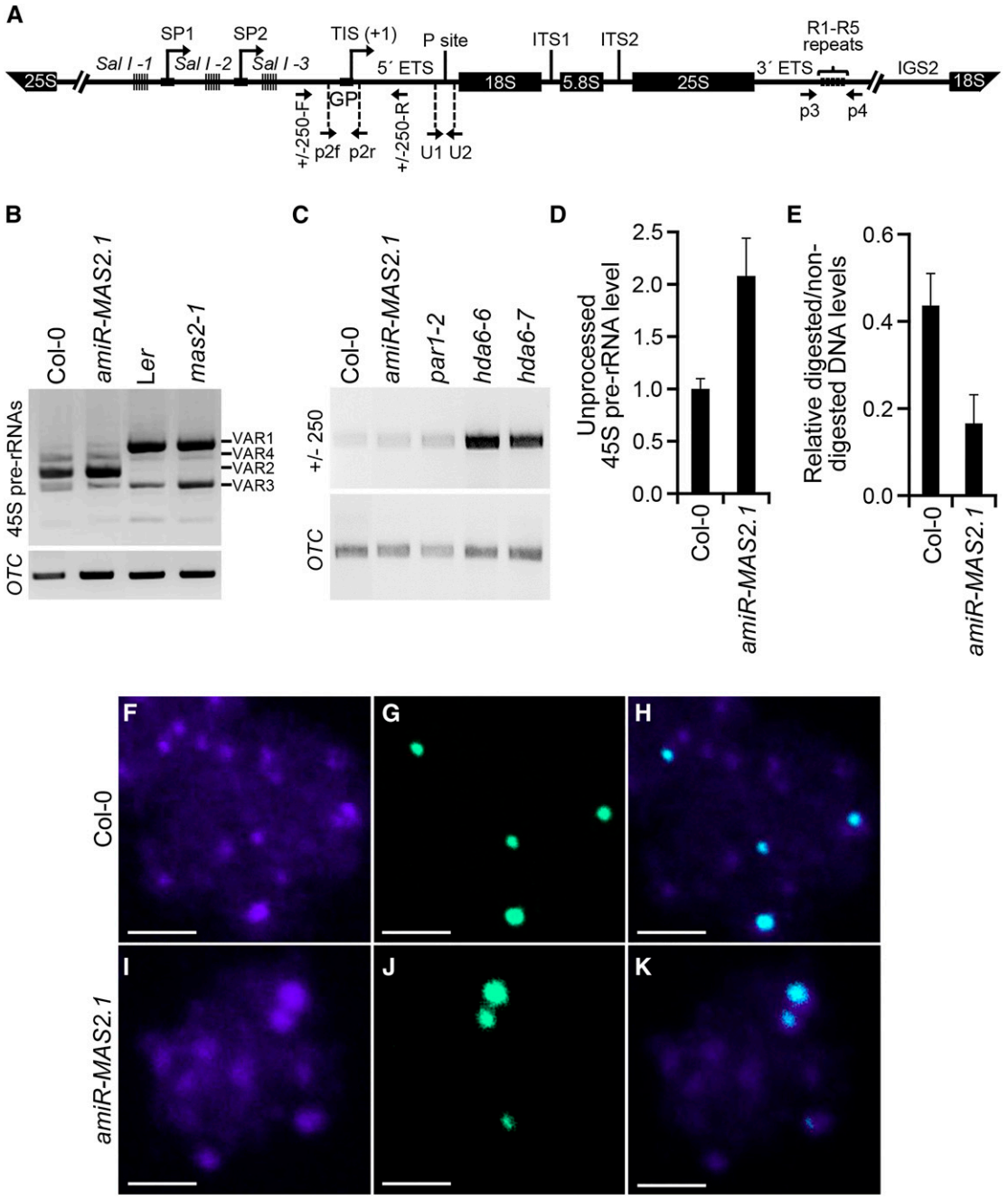

Figure 9. Effects of the *amiR-MAS2.1* Transgene on 45S Pre-rRNA Expression and NOR Condensation.

(A) Schematic representation of a 45S rDNA unit, modified from Pontvianne et al. (2010). GP, gene promoter; SP1 and SP2, spacer promoters; TIS, transcription initiation site. *Sal*I, repeat elements containing *Sal*I restriction sites. Upwards arrows with tip rightwards, transcription initiation sites. ITS1 and ITS2, internal transcribed spacers. Horizontal arrows indicate the positions of primers (not drawn to scale) used to detect pre-rRNA sequences.
(B) RT-PCR analysis of the expression of the VAR1-VAR4 45S rRNA variants in Col-0, *amiR-MAS2.1/amiR-MAS2.1*, L*er*, and *mas2-1/mas2-1* plants using the p3 and p4 primers (Supplemental Table 2).
(C) RT-PCR analysis of 45S pre-rRNA accumulation in Col-0, *amiR-MAS2.1/amiR-MAS2-1*, *parl1-2*, *hda6-6*, and *hda6-7* plants using the +/−250-F and +/−250-R primers.
(D) RT-qPCR analysis of unprocessed 45S pre-rRNAs in Col-0 and *amiR-MAS2.1/amiR-MAS2.1* plants using the U1 and U2 primers.
(E) Quantitative PCR analysis of 45S rDNA gene promoter methylation in Col-0 and *amiR-MAS2.1/amiR-MAS2.1* plants.
(D) and **(E)** Two biological replicas with three technical replicas each were performed. Error bars represent standard deviations.

In the *nuc-L1* and *hda6* mutants, NORs are decondensed (Probst et al., 2004; Pontvianne et al., 2007) and 45S pre-rRNA accumulates due to spurious transcription from the IGS region by Pol I and Pol II (Earley et al., 2010; Pontvianne et al., 2010), which in turn leads to the overproduction of small interfering RNAs (siRNAs) from the IGS region as a consequence of RNA-directed DNA methylation (Earley et al., 2010; Pontvianne et al., 2010). We also analyzed the accumulation of the 45S pre-rRNA transcripts produced by spurious transcription from the IGS region and the processing of these transcripts at the first step of cleavage (P site; Figure 9A). To amplify the 45S pre-rRNA, we used the +/−250-F and +/−250-R primers (Supplemental Table 2), which amplify the −250 to +250 region (Figure 9A; Earley et al., 2010). The 45S pre-rRNA processing was analyzed with the U1 + U2 primer pair (Supplemental Table 2), which amplify the sequences flanking the P site at the 5′ETS (Figure 9A; Shi et al., 2005). *amiR-MAS2.1/amiR-MAS2.1* and Col-0 plants accumulated comparable amounts of 45S pre-rRNA, while in *parl1-2* the level was far lower than that of *hda6* mutants (Figure 9C). Additionally, RT-qPCR analysis revealed that *amiR-MAS2.1/amiR-MAS2.1* plants accumulated approximately twice the amount of unprocessed 45S pre-rRNAs compared with Col-0 (Figure 9D). Mature rRNAs from processed 45S pre-rRNA were similar in *amiR-MAS2.1* and Col-0 plants (Supplemental Figure 21).

To study the effects of the silencing on NOR condensation, we analyzed NOR status in *amiR-MAS2.1/amiR-MAS2.1* plants by FISH assays, using a 45S rDNA probe (Sanchez Moran et al., 2001). Similar to the phenotype observed in *nuc-L1* and *hda6* mutants, we observed NOR decondensation in *amiR-MAS2.1* plants compared with Col-0 (Figures 9F to 9K).

amiR-MAS2.1 Affects Cytosine Methylation in the 45S Pre-rRNA 5′ETS

DNA methylation and histone modification epigenetically regulate the levels of rRNAs (Lawrence et al., 2004). Loss of *NUC-L1* and *HDA6* function in *nuc-L1* and *hda6* mutants leads to hypomethylation at the 5′ETS region affecting mainly the CG and, to a lesser extent, CHG contexts (where H indicates non-G nucleotides) (Earley et al., 2010; Pontvianne et al., 2010). To determine the DNA methylation status of the 5′ETS region in *amiR-MAS2.1* plants, we digested genomic DNA with the methylation-sensitive endonuclease *Hpa*II. Digested or non-digested DNA was used as template for quantitative PCR amplification using primers that flank the restriction sites (p2f and p2r) and hybridize downstream of the transcription initiation site (Figure 9A; Harscoët et al., 2010). We found that the ratio between digested and nondigested DNA was strongly reduced in *amiR-MAS2.1/amiR-MAS2.1* plants compared with Col-0 (Figure 9E), indicating that the promoter was hypomethylated in *amiR-MAS2.1/amiR-MAS2.1* plants, as occurred in the *nuc-L1* and *hda6* mutants.

DISCUSSION

Mutation of the SynMuv Domain of Arabidopsis MAS2 Causes Informational Suppression of *ago1* Alleles That Undergo Missplicing

The existence of SynMuv genes was first shown in *C. elegans* by screens for mutants deficient in vulval development (Ferguson and Horvitz, 1985, 1989; Ferguson et al., 1987; Howell and Rose, 1990). SynMuv genes act redundantly to prevent inappropriate vulval development (Horvitz and Sulston, 1980; Ferguson and Horvitz, 1989) and were initially classified into SynMuv A and B categories, based on their genetic interactions. SynMuv A and B single mutants are phenotypically wild type, but the AB double mutant combinations exhibit a synergistic, multivulva phenotype (Ferguson and Horvitz, 1989). Most SynMuv B genes encode epigenetic repressors, such as LHP1, the putative ortholog of Heterochromatin Protein 1, or are components of the NuRD (Nucleosome Remodeling Deacetylase) or DREAM (2DP, Retinoblastoma, E2F, and MuvB) repressor complexes (Saffer et al., 2011). The NuRD lysine deacetylase complex acts in a wide variety of cells (Yildirim et al., 2011), while DREAM is more specific and represses most cell cycle genes in mammalian quiescent G0 cells (Sadasivam and DeCaprio, 2013). Several genes encoding components of the splicing machinery behave as SynMuv B genes; their role in this process is still unknown (Ceron et al., 2007).

Second-site mutagenesis screens allow the identification of genes functionally related to a given gene of interest; the phenotype caused by a mutation can be modified, enhanced, or suppressed by a second-site mutation. One type of extragenic modifier that can be isolated by second-site mutagenesis is informational suppressors, mutations affecting any molecule involved in the transmission of information from DNA to protein (Prelich, 1999). Informational suppressors include those modifying pre-mRNA splicing, which suppress the splicing defects of some alleles of different genes. Some of these suppressors have helped in the elucidation of the regulation of alternative splicing in *C. elegans* (Hodgkin, 2005).

Here, we describe our characterization of the *MAS2* gene, which we identified from a second-site mutagenesis screen for suppressors of the morphological phenotype of *ago1-52*. *MAS2* is the putative Arabidopsis ortholog of human *NKAP* and *let-504* (*E01A2.4*), a SynMuv B gene of *C. elegans* (Poulin et al., 2005). MAS2 orthologs exist in almost all eukaryotes, and their sequence similarity is almost exclusively restricted to the SynMuv domain. NKAP family members encode nuclear proteins and, in most organisms except mammals, they exist as single-copy genes. Eight out the nine *mas2* suppressor mutations that we isolated affect conserved residues within the SynMuv domain; the remaining *mas2* mutation maps to another conserved region that seems to be exclusive to plants.

Figure 9. (continued).

(F) to **(K)** FISH assay. Representative mitotic prophase nuclei from Col-0 (**[F]** to **[H]**) and *amiR-MAS2.1* (**[I]** to **[K]**) cells. Fluorescent emissions are DAPI (**[F]** and **[I]**), hybridized 45S rDNA probe (**[G]** and **[J]**), and their overlay (**[H]** and **[K]**). Bars = 2.5 μm.

We found that *mas2* point alleles function as true extragenic suppressors of *ago1-52*, partially correcting *AGO1* missplicing in the *mas2 ago1-52* double mutants, hence increasing the ratio of AGO1 wild-type and mutant proteins. *mas2-1* also partially suppresses *ago1-51* missplicing. Immunoblot assays using an α-AGO1 antibody showed that the amount of wild-type AGO1 protein in *ago1-51* and *ago1-52* plants increased in the presence of *mas2-1* and decreased in the presence of the *amiR-MAS2.1* transgene.

Human NKAP interacts with pre-mRNAs and intronless mRNAs; it also interacts with FUSED IN SARCOMA (Burgute et al., 2014), a multifunctional protein involved in the regulation of alternative splicing and mRNA export from the nucleus to the cytoplasm. Taking together the recent results on human NKAP and our study of Arabidopsis MAS2, it seems plausible that NKAPs function in the regulation of the translation of aberrant or unspliced mRNAs, by regulating their nuclear export. This hypothesis provides an explanation for the observed suppression of *ago1-51* and *ago1-52* by the EMS-induced *mas2* alleles studied here, which seems to be due to partial correction of missplicing.

MAS2 Is an Essential Gene That Encodes a Multifunctional Protein

Whereas mammalian genes encoding NKAPs have been studied in some depth, little is known about NKAPs in *C. elegans* (LET-504) and Drosophila (CG6066). Human NKAP seems to be a multifunctional protein: It is a component of the Notch corepressor complex, it is required for proper T cell development (Pajerowski et al., 2009), and it plays an unknown role in splicing (Burgute et al., 2014).

Insertional disruption of the coding region of *MAS2* in the *mas2-2* and *mas2-3* lines caused embryonic lethality, as expected from the lethal phenotypes described for the lack-of-function mutations of *C. elegans*, Drosophila, and mammalian NKAP orthologs (Giot et al., 2003; Poulin et al., 2005; Pajerowski et al., 2009). The generation of transgenic plants carrying an artificial microRNA targeting *MAS2* mRNA allowed us to study the effects of the partial loss of function of *MAS2*; these plants displayed altered leaf morphology, early flowering, dwarfism, and partial loss of fertility. The embryonic lethality of *mas2-2* and *mas2-3* and the pleiotropic phenotype of *amiR-MAS2.1* plants indicate that *MAS2* is an essential gene required in multiple developmental processes.

MAS2 Is a Perinucleolar Protein That Interacts with Splicing and Ribosome Biogenesis Factors and Negatively Regulates 45S rRNA Expression

We found expression of *MAS2* was higher in cells undergoing active division, which require a continuous provision of proteins. MAS2 localized to the nucleus in a pattern that changed depending on the cell cycle: It was diffuse through the entire nucleus in actively dividing cells but became punctuate in differentiated cells. FISH analysis showed that MAS2 is a perinucleolar protein that colocalizes with the 45S rDNA genes.

The nucleolus is a multifunctional cellular compartment. In addition to ribosomal proteins, the Arabidopsis nucleolar proteome includes factors involved in mRNA biogenesis, splicing factors, and components of the exon-junction complex and the nonsense-mediated decay pathway, which participate in the degradation of aberrant mRNAs (Pendle et al., 2005). Aberrantly spliced mRNAs have been found to be enriched in the Arabidopsis nucleolus (Kim et al., 2009).

Perinucleolar localization of MAS2 is in agreement with our Y2H screen, which detected proteins predicted to function in nucleolar processes (Supplemental Table 3); this finding reinforces the hypothesis of a role for MAS2 in ribosome biogenesis and splicing. An indirect role for MAS2 in splicing is also plausible, as MAS2 interacts with factors directly acting in splicing or in regulation of splicing. MAS2 might also participate in mRNA quality control, preventing the translation of aberrant mRNAs. Further research will be required to analyze these possibilities.

The reduced methylation at the 45S rDNA promoters and the accumulation of unprocessed 45S pre-rRNAs observed in *amiR-MAS2.1* plants suggest that MAS2 participates in the regulation of 45S rDNA transcription and pre-45S rDNA processing. These molecular phenotypes are shared by the *nuc-L1* and *hda6* mutants; NUC-L1 and HDA6 participate in the silencing, transcription, and processing of 45S rDNA genes (Probst et al., 2004; Pontvianne et al., 2007; Earley et al., 2010; Pontvianne et al., 2010).

In addition, the similarity of the phenotype of *amiR-MAS2.1* plants and the phenotypes of mutants affecting ribosomal proteins and nucleolin as well as the synergistic interactions of *mas2* alleles and *nuc-L1* strongly suggest that MAS2 plays a key role in ribosome biogenesis together with or in parallel to nucleolin. The effects of *amiR-MAS2.1* on the methylation and accumulation of unprocessed 45S pre-rRNA were not as strong as those observed in the *nuc-L1* and *hda6* mutants, probably because *MAS2* expression is not completely abolished in *amiR-MAS2.1* plants.

NUC-L2 is a partially redundant paralog of *NUC-L1.* In contrast to the consequences of loss of function of *NUC-L1* and *MAS2*, loss of *NUC-L2* function causes hypermethylation of the 45S rDNA (Durut et al., 2014). Since our results suggest a functional relationship between *MAS2* and *NUC-L1*, and since loss of function of *NUC-L2* causes late flowering, a phenotype that is also opposite to that of *amiR-MAS2.1* plants, it should be interesting to examine whether MAS2 and NUC-L2 play antagonistic roles in the regulation of the expression of 45S rDNA and perhaps in the control of the transcription of other genes regulating flowering.

MAS2 and Human NKAP Likely Share DNA, RNA, and Protein Binding Preferences

Several lines of evidence indicate that MAS2 and human NKAP might share DNA, RNA, and protein binding preferences. A chromatin immunoprecipitation sequencing analysis revealed that human NKAP mainly binds to heterochromatic sequences, including those of centromeres (Burgute et al., 2014). Our FISH assays allowed us to visualize the colocalization of MAS2 and

the Arabidopsis NORs, which contain 45S rDNA linked to other heterochromatic regions, including the telomeric ends.

With regard to RNA binding preferences, several noncoding RNAs (ncRNAs), mainly small nucleolar RNAs and rRNAs, immunoprecipitate with human NKAP (Burgute et al., 2014). We did not carry out RNA binding assays, but we found that our suppressor *mas2* mutations modified the splicing and/or translational efficiency of the different *AGO1* or *ago1* mRNAs present in the *ago1-51* and *ago1-52* mutants. Additionally, MAS2 seems to be involved in the methylation of the promoters of 45S rDNA genes, which involves siRNAs (Earley et al., 2010). The SynMuv domain of human NKAP binds to RNA, and it has been suggested that the regulatory role of NKAP is mediated by its interaction with ncRNAs (Burgute et al., 2014). Due to the high sequence similarity between the SynMuv domains of MAS2 and human NKAP, we think it likely that MAS2 binds rRNAs, siRNAs, and other regulatory ncRNAs.

Finally, with regard to protein-protein interactions, human NKAP interacts with several types of RNA binding proteins, nuclear ribonuclear proteins, splicing factors, and RNA helicases involved in rRNA processing and splicing (Burgute et al., 2014). Our Y2H assays showed that MAS2 interacts with the previously mentioned classes of proteins (Supplemental Table 3). NKAP homologs have also been found in corepressor complexes in Drosophila and mammals. Drosophila CG6066 interacts with the ortholog of human CBF1-interacting corepressor (CIR) (CG6843) (Hsieh et al., 1999), a Notch corepressor complex component. NKAP associates with CIR and histone HDAC3 in human cells and its repressor activity depends on the interaction between its SynMuv domain and HDAC3 (Pajerowski et al., 2009). The Biological General Repository for Interaction Data sets (BioGRID; http://thebiogrid.org/; Stark et al., 2006) includes the interactions found in Y2H assays between E01A2.4, the *C. elegans* NKAP ortholog, and CIR-1 and the ribosomal protein RPL-22 (Boxem et al., 2008). In agreement with these results, we found that MAS2 physically interacts in a Y2H assay with a protein containing a CIR domain (encoded by At2g44200) and with the ribosomal protein RPS24B (Supplemental Table 3). Although we have not detected any physical interaction between MAS2 and any other protein with a known epigenetic role, our results suggest that MAS2 functions in both epigenetic regulation and splicing site selection or regulation of mRNA translation.

In conclusion, our study shows that MAS2, the single NKAP homolog present in the Arabidopsis genome, is a perinucleolar protein that colocalizes with 45S rDNA repeats and regulates 45S rRNA expression. The functional similarity between human NKAP and MAS2 seems to be very high. We consider that our work contributes to the characterization of a conserved factor that likely plays a key role in the regulation of plant gene expression.

METHODS

Plant Material and Growth Conditions

Arabidopsis thaliana L*er* and Col-0 wild-type accessions were obtained from the Nottingham Arabidopsis Stock Center (NASC) and then propagated at our institute for further analysis. Seeds of the SAIL_335_C06 and GABI_318G03 lines and the *parl1-2*, *hda6-6*, and *hda6-7* mutants were provided by NASC, and those of the CSHL_GT188551 line were provided by R. Martienssen. Seed sterilization and sowing, plant culture, and crosses were performed as previously described (Ponce et al., 1998; Berná et al., 1999). When required, culture media were supplemented with kanamycin (50 $\mu g \cdot mL^{-1}$), hygromycin (15 $\mu g \cdot mL^{-1}$), or Basta (5 $\mu g \cdot mL^{-1}$).

Positional Cloning and Molecular Characterization of *MAS2* and Its Mutant Alleles

Genomic DNA was extracted as described by Ponce et al. (2006). Fine mapping of the *mas2-1* mutation was performed by iterative linkage analysis as previously described (Ponce et al., 1999, 2006) using the primers listed in Supplemental Table 1. The *mas2* point mutations were identified by sequencing, using the At402720_F1, At402720_R1, At402720_F2, and At402720_R2 primers (Supplemental Table 2). Sequencing reactions and electrophoresis were performed with ABI PRISM BigDye Terminator Cycle Sequencing kits and on an ABI PRISM 3130xl Genetic Analyzer (Applied Biosystems), respectively. The presence of T-DNA insertions was verified by PCR using the SAIL_LB1 and At402720_R2 primers (SAIL_335_C06; *mas2-2*) and At402720_F1, Ds3_1, At402720_F1, and At402720_1R (CSHL_GT188551; *mas2-3*) primers (Supplemental Table 2). Discrimination between *MAS2* and *mas2-1* alleles was done by PCR amplification with At402720_F2 and At402720_R1 primers followed by digestion with *Bsa*HI, as the *mas2-1* mutation (GACGCC→GACACC) eliminates the *Bsa*HI restriction site.

RNA Isolation, Reverse Transcription, and RT-qPCR Analysis

Total RNA was isolated from 50 to 100 mg of rosettes with the TRI RNA isolation reagent (Sigma-Aldrich). Since *MAS2* lacks introns, prior to cDNA synthesis the RNA was treated with TURBO DNase (Ambion). Reverse transcription and RT-qPCR analyses were performed as described by Jover-Gil et al. (2012). RT-qPCR amplifications were performed on a Step-One Real-Time PCR System (Applied Biosystems). The *OTC* housekeeping gene (Quesada et al., 1999) was used as an internal control, as previously described (Cnops et al., 2004).

Construction of Transgenes and Transgenic Lines

To generate constructs for Gateway cloning, we performed PCR amplifications with the Phusion High-Fidelity DNA Polymerase (Finnzymes) and primers containing the attB1 (forward) or attB2 (reverse) sequences at their 5′ ends (Supplemental Table 2). Before being cloned into the pGEM-T Easy221 entry vector, PCR products were purified with the Illustra GFX PCR DNA and Gel Band Purification Kit (GE Healthcare Bio-Sciences). The entry and destination clones were obtained in 2.5-μL reactions using 1 μL of the BP and LR Clonase II kit (Life Technologies), respectively. Chemically competent *Escherichia coli* DH5α cells were transformed by the heat shock method; *Agrobacterium tumefaciens* C58C1 cells carrying the pSOUP helper plasmid were electroporated.

To obtain the $35S_{pro}$*:MAS2*, $35S_{pro}$*:mas2-1*, and $35S_{pro}$*:MAS2:GFP* overexpression constructs, the full-length coding sequences of *MAS2* and *mas2-1* were PCR amplified from L*er* and *ago1-52 mas2-1* plants, respectively. The destination vector pMDC32 was used for $35S_{pro}$*:MAS2* and $35S_{pro}$*:mas2-1*, and pMDC85 for $35S_{pro}$*:MAS2:GFP*. A 1.1-kb DNA region upstream of the translation start codon of the *MAS2* gene was used as promoter in the $MAS2_{pro}$*:GUS* and $MAS2_{pro}$*:MAS2:GFP* constructs. The fragments were obtained by PCR and subcloned into the pMDC162 and pMDC111 destination vectors, respectively. To obtain GFP translational fusions, the coding regions of *MAS2* and *mas2-1* lacking their stop codons were PCR amplified from L*er* and *ago1-52 mas2-1* plants,

respectively. All constructs were sequence verified before being transferred into plants, which was performed by the floral dip method (Clough and Bent, 1998). Primers used for obtaining these constructs and for sequencing them are described in Supplemental Table 2.

Arabidopsis transgenic lines expressing the *amiR-MAS2* artificial microRNA (5′-UAUACGUUUACCUUGCUGGAC-3′) were obtained as described in Jover-Gil et al. (2014).

Plant Gross Morphology and Histology, and Histochemical Assays

Leaf venation diagrams were obtained from first- and third-node leaves as described previously (Candela et al., 1999; Alonso-Peral et al., 2006). For histological analyses, first- and third-node leaves were fixed with FAA/Triton (1.85% formaldehyde, 45% ethanol, 5% acetic acid, and 1% Triton X-100) as described by Serrano-Cartagena et al. (2000). After dehydration, tissues were embedded in Technovit 7100 resin (Heraeus Kulzer) following the manufacturer's instructions. Sections of 7-mm thickness were cut on a Microm International HM350S microtome and stained with 0.1% (w/v) Toluidine blue. GUS assays were performed as described by Robles et al. (2010). In vivo visualization of MAS2 subcellular localization was performed in root cells of plants carrying MAS2-GFP fusion proteins. For nuclear staining, plant tissue was submerged in 1 $\mu g \cdot mL^{-1}$ DAPI for 30 s and then rinsed in water. Micrographs were taken on a Nikon D-Eclipse C1 confocal microscope.

Immunoblot Assay

Proteins were extracted with TRI reagent (Sigma-Aldrich) from 50 to 100 mg of material of plants collected at 15 DAS, precipitated with isopropanol, washed three times with 0.3 M guanidine-HCl (96% ethanol), and resuspended into resuspension buffer (8 M urea, 40 mM Tris-HCl, pH 6.8, 0.1 mM EDTA, and 1% SDS). Each protein extract (160 µg) was loaded in a 7% polyacrylamide gel. SDS-PAGE and electrotransfer to nitrocellulose were performed as previously described (Esteve-Bruna et al., 2013). Two primary antibodies were used: against AGO1 (Agrisera; AS09 527P) at 1:500 dilution and against the large subunit of Rubisco (Agrisera; AS03 037) at 1:500 to 1:2500 dilution.

FISH

Tissue preparation and FISH were performed as previously described (Armstrong and Hultén, 1998; Fransz et al., 1998; Sanchez Moran et al., 2001) with minor modifications. Flower buds were collected into a 50-mL Falcon tube and kept in ice-cold water at 4°C for 64 h to accumulate cells in mitotic metaphase. After three washes in citrate buffer (pH 4.5), tissue was incubated with a mixture of 2% (w/v) Cellulase Onozuka R-10 and 2% (w/v) Macerozyme R-10 (Duchefa Biochemie) in citrate buffer at 37°C for 2 h in a humid hybridization chamber before being macerated with a needle. A biotin-labeled 45S rDNA probe (pTa71; Gerlach and Bedbrook, 1979) and a 1:260 dilution of streptavidin-Cy3 (Roche) antibody in TNB buffer (100 mM Tris-HCl, pH 7.5, 150 mM NaCl, and 0.5% nonfat dry milk as a blocking reagent) were used. Confocal laser scanning microscopy images were obtained and digitally processed using the EZ-C1 operation software for a Nikon D-Eclipse C1 microscope.

Analysis of the Methylation Status of the 45S rDNA Promoter

Genomic DNA was extracted and digested with the methylation-sensitive *Hpa*II restriction endonuclease. Cleavage by *Hpa*II of the 5′-CCGG-3′ tetranucleotide is blocked by the presence of 5-MeC at this site (5′-C^{me}CGG-3′). Digested and nondigested DNA was used as template for quantitative PCR amplifications using the p2f and p2r primers, which flank the restriction sites (Supplemental Table 2; Harscoët et al., 2010). The 25S rRNA gene was amplified with the 25SrRNA_F/R primer set and used as an endogenous control for quantitative PCR experiments. Bars represent the ratio between levels of PCR amplification products representing digested and nondigested fragments.

Accession Numbers

Sequence data from this article can be found in The Arabidopsis Information Resource (http://www.arabidopsis.org/) under the following accession numbers: *MAS2* (At4g02720), *AGO1* (At1g48410), *NUC-L1* (At1g48920), and *HDA6* (At5g63110).

Supplemental Data

Supplemental Figure 1. Positional cloning of the *MAS2* gene.

Supplemental Figure 2. Molecular nature and position of *mas2* point mutations.

Supplemental Figure 3. Sequence conservation among eukaryotic NKAPs.

Supplemental Figure 4. Sequence conservation among plant NKAPs.

Supplemental Figure 5. *ago1* alleles used in this work.

Supplemental Figure 6. Morphological phenotype of *ago1-51 mas2-1* adult plants.

Supplemental Figure 7. Effects of the *mas2* mutations on the levels of *AGO1* splice variants.

Supplemental Figure 8. Visualization of AGO1 protein isoforms in *ago1* mutants.

Supplemental Figure 9. Phenotypic effects of the overexpression of *MAS2* and *mas2-1* on the L*er*, *ago1-51*, and *ago1-52* backgrounds at the rosette stage.

Supplemental Figure 10. Phenotypic effects of the overexpression of *mas2-1* on the *ago1-52* background in adult plants.

Supplemental Figure 11. Phenotypic effects of the overexpression of *mas2-1* on the *ago1-51* background in adult plants.

Supplemental Figure 12. Analysis of the of GABI_318G03 insertional line.

Supplemental Figure 13. Seeds and embryos of *MAS2*/*mas2-2* plants.

Supplemental Figure 14. Morphological phenotypes caused by the *amiR-MAS2* transgene in different genetic backgrounds.

Supplemental Figure 15. Histology of *amiR-MAS2.1* leaves.

Supplemental Figure 16. Levels of the *AGO1* splice variants in *ago1-52 amiR-MAS2.1* plants.

Supplemental Figure 17. Visualization of $MAS2_{pro}$*:GUS* activity in wild-type plants.

Supplemental Figure 18. Spatial pattern of expression of *MAS2*.

Supplemental Figure 19. Subcellular localization of the MAS2:GFP and MAS2-1:GFP proteins.

Supplemental Figure 20. Subcellular localization of the MAS2:GFP protein in cells of the root elongation zone from homozygous $35S_{pro}$*:MAS2:GFP* plants.

Supplemental Figure 21. Effects of *amiR-MAS2.1* on 45S rRNA processing.

Supplemental Table 1. Primer sets used for the fine mapping of *MAS2*.

Supplemental Table 2. Other primer sets used in this work.

Supplemental Table 3. Results of a Y2H-based screen using MAS2 as a bait.

Supplemental References.

ACKNOWLEDGMENTS

We thank R. Sarmiento-Mañús, J.M. Serrano, F.M. Lozano, T. Trujillo, and D. Navarro for their excellent technical assistance, J.L. Santos, M. Pradillo, and F.J. Medina for their help and advice, J.L. Micol for useful discussions and comments on the article as well as for the use of his facilities, B. Scheres for the pGEM-T Easy221 vector, and J. Simorowski and R. Martienssen for the CSHL_GT188551 line. This research was supported by grants from the Ministerio de Economía y Competitividad of Spain (BIO2008-01900 and BIO2014-56889-R) and the Generalitat Valenciana (PROMETEO/2009/112 and PROMETEOII/2014/006) to M.R.P.

AUTHOR CONTRIBUTIONS

M.R.P. conceived and designed research. M.R.P., A.B.S.-G., V.A., R.M.-P., and S.J.-G. performed research and analyzed data. M.R.P., R.M.-P., S.J.-G., and A.B.S.-G. wrote the article.

Received February 12, 2015; revised June 2, 2015; accepted June 12, 2015; published July 2, 2015.

REFERENCES

Abou-Ellail, M., Cooke, R., and Sáez-Vásquez, J. (2011). Variations in a team: major and minor variants of *Arabidopsis thaliana* rDNA genes. Nucleus **2:** 294–299.

Alonso-Peral, M.M., Candela, H., del Pozo, J.C., Martínez-Laborda, A., Ponce, M.R., and Micol, J.L. (2006). The *HVE/CAND1* gene is required for the early patterning of leaf venation in Arabidopsis. Development **133:** 3755–3766.

Arabidopsis Interactome Mapping Consortium (2011). Evidence for network evolution in an Arabidopsis interactome map. Science **333:** 601–607.

Armstrong, S.J., and Hultén, M.A. (1998). Meiotic segregation analysis by FISH investigations in sperm and spermatocytes of translocation heterozygotes. Eur. J. Hum. Genet. **6:** 430–431.

Bartel, D.P. (2009). MicroRNAs: target recognition and regulatory functions. Cell **136:** 215–233.

Berná, G., Robles, P., and Micol, J.L. (1999). A mutational analysis of leaf morphogenesis in *Arabidopsis thaliana.* Genetics **152:** 729–742.

Bessonov, S., Anokhina, M., Will, C.L., Urlaub, H., and Lührmann, R. (2008). Isolation of an active step I spliceosome and composition of its RNP core. Nature **452:** 846–850.

Bessonov, S., Anokhina, M., Krasauskas, A., Golas, M.M., Sander, B., Will, C.L., Urlaub, H., Stark, H., and Lührmann, R. (2010). Characterization of purified human Bact spliceosomal complexes reveals compositional and morphological changes during spliceosome activation and first step catalysis. RNA **16:** 2384–2403.

Bohmert, K., Camus, I., Bellini, C., Bouchez, D., Caboche, M., and Benning, C. (1998). *AGO1* defines a novel locus of *Arabidopsis* controlling leaf development. EMBO J. **17:** 170–180.

Boxem, M., et al. (2008). A protein domain-based interactome network for *C. elegans* early embryogenesis. Cell **134:** 534–545.

Bray, S.J. (2006). Notch signalling: a simple pathway becomes complex. Nat. Rev. Mol. Cell Biol. **7:** 678–689.

Burgute, B.D., Peche, V.S., Steckelberg, A.L., Glöckner, G., Gaßen, B., Gehring, N.H., and Noegel, A.A. (2014). NKAP is a novel RS-related protein that interacts with RNA and RNA binding proteins. Nucleic Acids Res. **42:** 3177–3193.

Campbell, D.A. (1992). *Bodo caudatus* medRNA and 5S rRNA genes: tandem arrangement and phylogenetic analyses. Biochem. Biophys. Res. Commun. **182:** 1053–1058.

Candela, H., Martínez-Laborda, A., and Micol, J.L. (1999). Venation pattern formation in *Arabidopsis thaliana* vegetative leaves. Dev. Biol. **205:** 205–216.

Casanova-Sáez, R., Candela, H., and Micol, J.L. (2014). Combined haploinsufficiency and purifying selection drive retention of *RPL36a* paralogs in Arabidopsis. Sci. Rep. **4:** 4122.

Ceron, J., Rual, J.F., Chandra, A., Dupuy, D., Vidal, M., and van den Heuvel, S. (2007). Large-scale RNAi screens identify novel genes that interact with the *C. elegans* retinoblastoma pathway as well as splicing-related components with synMuv B activity. BMC Dev. Biol. **7:** 30–45.

Chen, D., Li, Z., Yang, Q., Zhang, J., Zhai, Z., and Shu, H.B. (2003). Identification of a nuclear protein that promotes NF-kappaB activation. Biochem. Biophys. Res. Commun. **310:** 720–724.

Cheng, N.H., Liu, J.Z., Nelson, R.S., and Hirschi, K.D. (2004). Characterization of CXIP4, a novel *Arabidopsis* protein that activates the H^+/Ca^{2+} antiporter, CAX1. FEBS Lett. **559:** 99–106.

Cloix, C., Tutois, S., Yukawa, Y., Mathieu, O., Cuvillier, C., Espagnol, M.C., Picard, G., and Tourmente, S. (2002). Analysis of the 5S RNA pool in *Arabidopsis thaliana*: RNAs are heterogeneous and only two of the genomic 5S loci produce mature 5S RNA. Genome Res. **12:** 132–144.

Clough, S.J., and Bent, A.F. (1998). Floral dip: a simplified method for *Agrobacterium*-mediated transformation of *Arabidopsis thaliana.* Plant J. **16:** 735–743.

Cnops, G., Jover-Gil, S., Peters, J.L., Neyt, P., De Block, S., Robles, P., Ponce, M.R., Gerats, T., Micol, J.L., and Van Lijsebettens, M. (2004). The *rotunda2* mutants identify a role for the *LEUNIG* gene in vegetative leaf morphogenesis. J. Exp. Bot. **55:** 1529–1539.

Costa-Nunes, P., Pontes, O., Preuss, S.B., and Pikaard, C.S. (2010). Extra views on RNA-dependent DNA methylation and MBD6-dependent heterochromatin formation in nucleolar dominance. Nucleus **1:** 254–259.

Creff, A., Sormani, R., and Desnos, T. (2010). The two Arabidopsis *RPS6* genes, encoding for cytoplasmic ribosomal proteins S6, are functionally equivalent. Plant Mol. Biol. **73:** 533–546.

Durut, N., et al. (2014). A duplicated *NUCLEOLIN* gene with antagonistic activity is required for chromatin organization of silent 45S rDNA in Arabidopsis. Plant Cell **26:** 1330–1344.

Earley, K.W., Pontvianne, F., Wierzbicki, A.T., Blevins, T., Tucker, S., Costa-Nunes, P., Pontes, O., and Pikaard, C.S. (2010). Mechanisms of HDA6-mediated rRNA gene silencing: suppression of intergenic Pol II transcription and differential effects on maintenance versus siRNA-directed cytosine methylation. Genes Dev. **24:** 1119–1132.

Esteve-Bruna, D., Pérez-Pérez, J.M., Ponce, M.R., and Micol, J.L. (2013). *incurvata13*, a novel allele of *AUXIN RESISTANT6*, reveals a specific role for auxin and the SCF complex in Arabidopsis embryogenesis, vascular specification, and leaf flatness. Plant Physiol. **161:** 1303–1320.

Ferguson, E.L., and Horvitz, H.R. (1985). Identification and characterization of 22 genes that affect the vulval cell lineages of the nematode *Caenorhabditis elegans.* Genetics **110:** 17–72.

Ferguson, E.L., and Horvitz, H.R. (1989). The multivulva phenotype of certain *Caenorhabditis elegans* mutants results from defects in two functionally redundant pathways. Genetics **123:** 109–121.

Ferguson, E.L., Sternberg, P.W., and Horvitz, H.R. (1987). A genetic pathway for the specification of the vulval cell lineages of *Caenorhabditis elegans.* Nature **326:** 259–267.

Fernández-Nohales, P., Domenech, M.J., Martínez de Alba, A.E., Micol, J.L., Ponce, M.R., and Madueño, F. (2014). AGO1 controls arabidopsis inflorescence architecture possibly by regulating *TFL1* expression. Ann. Bot. (Lond.) **114:** 1471–1481.

Fransz, P., Armstrong, S., Alonso-Blanco, C., Fischer, T.C., Torres-Ruiz, R.A., and Jones, G. (1998). Cytogenetics for the model system *Arabidopsis thaliana.* Plant J. **13:** 867–876.

Gerlach, W.L., and Bedbrook, J.R. (1979). Cloning and characterization of ribosomal RNA genes from wheat and barley. Nucleic Acids Res. **7:** 1869–1885.

Giot, L., et al. (2003). A protein interaction map of *Drosophila melanogaster.* Science **302:** 1727–1736.

Granato, D.C., Machado-Santelli, G.M., and Oliveira, C.C. (2008). Nop53p interacts with 5.8S rRNA co-transcriptionally, and regulates processing of pre-rRNA by the exosome. FEBS J. **275:** 4164–4178.

Gruendler, P., Unfried, I., Pointner, R., and Schweizer, D. (1989). Nucleotide sequence of the 25S-18S ribosomal gene spacer from *Arabidopsis thaliana.* Nucleic Acids Res. **17:** 6395–6396.

Gruendler, P., Unfried, I., Pascher, K., and Schweizer, D. (1991). rDNA intergenic region from *Arabidopsis thaliana*. Structural analysis, intraspecific variation and functional implications. J. Mol. Biol. **221:** 1209–1222.

Grummt, I. (2003). Life on a planet of its own: regulation of RNA polymerase I transcription in the nucleolus. Genes Dev. **17:** 1691–1702.

Guan, Q., Wu, J., Zhang, Y., Jiang, C., Liu, R., Chai, C., and Zhu, J. (2013). A DEAD box RNA helicase is critical for pre-mRNA splicing, cold-responsive gene regulation, and cold tolerance in *Arabidopsis.* Plant Cell **25:** 342–356.

Harscoët, E., Dubreucq, B., Palauqui, J.C., and Lepiniec, L. (2010). *NOF1* encodes an Arabidopsis protein involved in the control of rRNA expression. PLoS ONE **5:** e12829.

He, D., Fiz-Palacios, O., Fu, C.J., Fehling, J., Tsai, C.C., and Baldauf, S.L. (2014). An alternative root for the eukaryote tree of life. Curr. Biol. **24:** 465–470.

Hodgkin, J. (2005). Genetic suppression. In WormBook: The Online Review of *C. elegans* Biology, doi/10.1895/wormbook.1.59.1.

Horiguchi, G., Mollá-Morales, A., Pérez-Pérez, J.M., Kojima, K., Robles, P., Ponce, M.R., Micol, J.L., and Tsukaya, H. (2011). Differential contributions of ribosomal protein genes to *Arabidopsis thaliana* leaf development. Plant J. **65:** 724–736.

Horvitz, H.R., and Sulston, J.E. (1980). Isolation and genetic characterization of cell-lineage mutants of the nematode *Caenorhabditis elegans.* Genetics **96:** 435–454.

Howell, A.M., and Rose, A.M. (1990). Essential genes in the *hDf6* region of chromosome I in *Caenorhabditis elegans.* Genetics **126:** 583–592.

Hsieh, J.J., Zhou, S., Chen, L., Young, D.B., and Hayward, S.D. (1999). CIR, a corepressor linking the DNA binding factor CBF1 to the histone deacetylase complex. Proc. Natl. Acad. Sci. USA **96:** 23–28.

Ilagan, J.O., Chalkley, R.J., Burlingame, A.L., and Jurica, M.S. (2013). Rearrangements within human spliceosomes captured after exon ligation. RNA **19:** 400–412.

Ito, T., Kim, G.T., and Shinozaki, K. (2000). Disruption of an *Arabidopsis* cytoplasmic ribosomal protein S13-homologous gene by transposon-mediated mutagenesis causes aberrant growth and development. Plant J. **22:** 257–264.

Jones-Rhoades, M.W., Bartel, D.P., and Bartel, B. (2006). MicroRNAS and their regulatory roles in plants. Annu. Rev. Plant Biol. **57:** 19–53.

Jover-Gil, S., Candela, H., and Ponce, M.R. (2005). Plant microRNAs and development. Int. J. Dev. Biol. **49:** 733–744.

Jover-Gil, S., Candela, H., Robles, P., Aguilera, V., Barrero, J.M., Micol, J.L., and Ponce, M.R. (2012). The microRNA pathway genes *AGO1, HEN1* and *HYL1* participate in leaf proximal-distal, venation and stomatal patterning in Arabidopsis. Plant Cell Physiol. **53:** 1322–1333.

Jover-Gil, S., Paz-Ares, J., Micol, J.L., and Ponce, M.R. (2014). Multi-gene silencing in Arabidopsis: a collection of artificial microRNAs targeting groups of paralogs encoding transcription factors. Plant J. **80:** 149–160.

Jurica, M.S., and Moore, M.J. (2002). Capturing splicing complexes to study structure and mechanism. Methods **28:** 336–345.

Kim, S.H., Koroleva, O.A., Lewandowska, D., Pendle, A.F., Clark, G.P., Simpson, C.G., Shaw, P.J., and Brown, J.W. (2009). Aberrant mRNA transcripts and the nonsense-mediated decay proteins UPF2 and UPF3 are enriched in the Arabidopsis nucleolus. Plant Cell **21:** 2045–2057.

Laferté, A., Favry, E., Sentenac, A., Riva, M., Carles, C., and Chédin, S. (2006). The transcriptional activity of RNA polymerase I is a key determinant for the level of all ribosome components. Genes Dev. **20:** 2030–2040.

Lam, S.Y., Horn, S.R., Radford, S.J., Housworth, E.A., Stahl, F.W., and Copenhaver, G.P. (2005). Crossover interference on nucleolus organizing region-bearing chromosomes in Arabidopsis. Genetics **170:** 807–812.

Lawrence, R.J., Earley, K., Pontes, O., Silva, M., Chen, Z.J., Neves, N., Viegas, W., and Pikaard, C.S. (2004). A concerted DNA methylation/histone methylation switch regulates rRNA gene dosage control and nucleolar dominance. Mol. Cell **13:** 599–609.

Layat, E., Sáez-Vásquez, J., and Tourmente, S. (2012). Regulation of Pol I-transcribed 45S rDNA and Pol III-transcribed 5S rDNA in Arabidopsis. Plant Cell Physiol. **53:** 267–276.

Luo, L., Ando, S., Sasabe, M., Machida, C., Kurihara, D., Higashiyama, T., and Machida, Y. (2012). Arabidopsis ASYMMETRIC LEAVES2 protein required for leaf morphogenesis consistently forms speckles during mitosis of tobacco BY-2 cells via signals in its specific sequence. J. Plant Res. **125:** 661–668.

Mallory, A., and Vaucheret, H. (2010). Form, function, and regulation of ARGONAUTE proteins. Plant Cell **22:** 3879–3889.

Micol-Ponce, R., Aguilera, V., and Ponce, M.R. (2014). A genetic screen for suppressors of a hypomorphic allele of Arabidopsis *ARGONAUTE1.* Sci. Rep. **4:** 5533.

Morel, J.B., Godon, C., Mourrain, P., Béclin, C., Boutet, S., Feuerbach, F., Proux, F., and Vaucheret, H. (2002). Fertile hypomorphic *ARGONAUTE* (*ago1*) mutants impaired in post-transcriptional gene silencing and virus resistance. Plant Cell **14:** 629–639.

Murfett, J., Wang, X.J., Hagen, G., and Guilfoyle, T.J. (2001). Identification of Arabidopsis histone deacetylase HDA6 mutants that affect transgene expression. Plant Cell **13:** 1047–1061.

Pajerowski, A.G., Nguyen, C., Aghajanian, H., Shapiro, M.J., and Shapiro, V.S. (2009). NKAP is a transcriptional repressor of notch signaling and is required for T cell development. Immunity **30:** 696–707.

Pendle, A.F., Clark, G.P., Boon, R., Lewandowska, D., Lam, Y.W., Andersen, J., Mann, M., Lamond, A.I., Brown, J.W., and Shaw, P.J. (2005). Proteomic analysis of the Arabidopsis nucleolus suggests novel nucleolar functions. Mol. Biol. Cell **16:** 260–269.

Petricka, J.J., and Nelson, T.M. (2007). Arabidopsis nucleolin affects plant development and patterning. Plant Physiol. **144:** 173–186.

Ponce, M.R., Quesada, V., and Micol, J.L. (1998). Rapid discrimination of sequences flanking and within T-DNA insertions in the *Arabidopsis* genome. Plant J. **14:** 497–501.

Ponce, M.R., Robles, P., and Micol, J.L. (1999). High-throughput genetic mapping in *Arabidopsis thaliana.* Mol. Gen. Genet. **261:** 408–415.

Ponce, M.R., Robles, P., Lozano, F.M., Brotóns, M.A., and Micol, J.L. (2006). Low-resolution mapping of untagged mutations. Methods Mol. Biol. **323:** 105–113.

Pontvianne, F., Matía, I., Douet, J., Tourmente, S., Medina, F.J., Echeverria, M., and Sáez-Vásquez, J. (2007). Characterization of *AtNUC-L1* reveals a central role of nucleolin in nucleolus organization and silencing of *AtNUC-L2* gene in *Arabidopsis.* Mol. Biol. Cell **18:** 369–379.

Pontvianne, F., et al. (2010). Nucleolin is required for DNA methylation state and the expression of rRNA gene variants in *Arabidopsis thaliana.* PLoS Genet. **6:** e1001225.

Poulin, G., Dong, Y., Fraser, A.G., Hopper, N.A., and Ahringer, J. (2005). Chromatin regulation and sumoylation in the inhibition of Ras-induced vulval development in *Caenorhabditis elegans.* EMBO J. **24:** 2613–2623.

Prelich, G. (1999). Suppression mechanisms: themes from variations. Trends Genet. **15:** 261–266.

Probst, A.V., Fagard, M., Proux, F., Mourrain, P., Boutet, S., Earley, K., Lawrence, R.J., Pikaard, C.S., Murfett, J., Furner, I., Vaucheret, H., and Mittelsten Scheid, O. (2004). Arabidopsis histone deacetylase *HDA6* is required for maintenance of transcriptional gene silencing and determines nuclear organization of rDNA repeats. Plant Cell **16:** 1021–1034.

Quesada, V., Ponce, M.R., and Micol, J.L. (1999). *OTC* and *AUL1*, two convergent and overlapping genes in the nuclear genome of *Arabidopsis thaliana.* FEBS Lett. **461:** 101–106.

Rogers, K., and Chen, X. (2013). Biogenesis, turnover, and mode of action of plant microRNAs. Plant Cell **25:** 2383–2399.

Robles, P., Fleury, D., Candela, H., Cnops, G., Alonso-Peral, M.M., Anami, S., Falcone, A., Caldana, C., Willmitzer, L., Ponce, M.R., Van Lijsebettens, M., and Micol, J.L. (2010). The *RON1/FRY1/SAL1* gene is required for leaf morphogenesis and venation patterning in Arabidopsis. Plant Physiol. **152:** 1357–1372.

Sadasivam, S., and DeCaprio, J.A. (2013). The DREAM complex: master coordinator of cell cycle-dependent gene expression. Nat. Rev. Cancer **13:** 585–595.

Saffer, A.M., Kim, D.H., van Oudenaarden, A., and Horvitz, H.R. (2011). The *Caenorhabditis elegans* synthetic multivulva genes prevent ras pathway activation by tightly repressing global ectopic expression of *lin-3* EGF. PLoS Genet. **7:** e1002418.

Sanchez Moran, E., Armstrong, S.J., Santos, J.L., Franklin, F.C., and Jones, G.H. (2001). Chiasma formation in *Arabidopsis thaliana* accession Wassilewskija and in two meiotic mutants. Chromosome Res. **9:** 121–128.

Schwacke, R., Schneider, A., van der Graaff, E., Fischer, K., Catoni, E., Desimone, M., Frommer, W.B., Flügge, U.I., and Kunze, R. (2003). ARAMEMNON, a novel database for Arabidopsis integral membrane proteins. Plant Physiol. **131:** 16–26.

Serrano-Cartagena, J., Candela, H., Robles, P., Ponce, M.R., Pérez-Pérez, J.M., Piqueras, P., and Micol, J.L. (2000). Genetic analysis of *incurvata* mutants reveals three independent genetic operations at work in Arabidopsis leaf morphogenesis. Genetics **156:** 1363–1377.

Shi, D.Q., Liu, J., Xiang, Y.H., Ye, D., Sundaresan, V., and Yang, W.C. (2005). *SLOW WALKER1*, essential for gametogenesis in Arabidopsis, encodes a WD40 protein involved in 18S ribosomal RNA biogenesis. Plant Cell **17:** 2340–2354.

Stark, C., Breitkreutz, B.J., Reguly, T., Boucher, L., Breitkreutz, A., and Tyers, M. (2006). BioGRID: a general repository for interaction datasets. Nucleic Acids Res. **34:** D535–D539.

Unfried, I., Stocker, U., and Gruendler, P. (1989). Nucleotide sequence of the 18S rRNA gene from *Arabidopsis thaliana* Col-0. Nucleic Acids Res. **17:** 7513.

Van Lijsebettens, M., Vanderhaeghen, R., De Block, M., Bauw, G., Villarroel, R., and Van Montagu, M. (1994). An S18 ribosomal protein gene copy at the *Arabidopsis PFL* locus affects plant development by its specific expression in meristems. EMBO J. **13:** 3378–3388.

Voinnet, O. (2009). Origin, biogenesis, and activity of plant microRNAs. Cell **136:** 669–687.

Yildirim, O., Li, R., Hung, J.H., Chen, P.B., Dong, X., Ee, L.S., Weng, Z., Rando, O.J., and Fazzio, T.G. (2011). Mbd3/NURD complex regulates expression of 5-hydroxymethylcytosine marked genes in embryonic stem cells. Cell **147:** 1498–1510.